

Manuscript Number: POWER-D-18-03124R3

Title: Template Electrodeposition and Characterization of Nanostructured Pb as a Negative Electrode for Lead-Acid Battery

Article Type: Research Paper

Keywords: Lead nanowires, template electrodeposition, lead-acid battery, nanostructures, cycling efficiency, high C-rate cycling

Corresponding Author: Professor Rosalinda Inguanta, Assistant Professor

Corresponding Author's Institution: Università di Palermo

First Author: Maria Grazia Insinga, PhD Student

Order of Authors: Maria Grazia Insinga, PhD Student; Roberto Luigi Oliveri, Dott; Carmelo Sunseri, prof; Rosalinda Inguanta, Assistant Professor

Abstract: Despite Lead Acid Battery (LAB) is the oldest electrochemical energy storage system, diffusion in the emerging sectors of technological interest is inhibited by its drawbacks. The principal ones are low energy density and negative plate sulphating on high rate discharging. In this work, it is shown the possibility of overcoming such drawbacks by using nanostructured lead as a negative electrode. Lead nanowires (NWs) were fabricated by electrochemical deposition in template, which is an easy, cheap, and easily scalable process. Their morphology and crystal structure have been characterized by electron microscopy and X-ray diffraction, respectively. An electrochemical cell simulating LAB has been assembled with PbO<sub>2</sub> as a counter electrode and an AGM separator, both from commercial battery. Cycling tests were conducted at 10C-rate, setting the cut-off voltage on discharging at 1.2 V. For comparison, also cycling tests at 1C-rate have been carried out, in otherwise identical conditions. At both C-rates, performances in terms of cycling efficiency and lifetime were found a lot better than those of current LABs. The high porosity formed under cycling at 10C-rate provides a reliable explanation of the results.

## Response to Reviewers

### *Reviewer #1*

- 1. Comment:** The morphology shows great changed before and after the cycling. This may indicate the changes either in porosity or in structure take place. As the authors said, they believe that the porosity is the key factor for the electrode performances, and discussed much on it. However, we still did not know what the exact meaning of porosity and how the porosity changes clearly with sufficient evidences. Therefore, the authors should exhibit more evidences on the porosity and the changes in porosity in different stages. Otherwise, it is doubtful that the porosity maintains a positively relationship with the electrode performance. In addition, the explanations on the performances under different C-rates seem not to be convincing.

**Response:** According to the referee's criticism, the manuscript has been substantially amended about the probable cause determining the performances of the nanostructured lead as a negative electrode of an electrochemical cell simulating a Lead Acid Battery. Since the referee has doubts as to the porosity enhancement over cycling, we have added i) new results on the wettability of the surface, and ii) new SEM images showing the surface morphology after different cycles. We hope that these modifications are enough to provide a likely explanation of the observed behaviour. As it is usual for all researchers, they are engaged in looking for a sound explanation of the experiments, never for the truth. We think to have done so also in the present case.

In particular, in the Experimental section we have added the information regarding angle contact measurements (at pag 5) while at pag. 11 of manuscript we have inserted the following paragraph:

“Figures 6 and 7 clearly indicate that when electrodeposited nanostructured lead is employed as a negative electrode in a cell simulating a LAB, not only electrode polarization

decreases but also efficiency improves under cycling and with C-rate. These findings are different in comparison with the behaviour of current commercial LABs pasted electrodes which decay rapidly if cycled under the stressing conditions selected for testing nanostructured electrodes. In this context, it is mandatory to scrutinize the possible causes of such behaviour.

At this aim, dedicated investigations were conducted. First of all, the wettability of the nanostructured electrode was determined. Figure 8a shows the contact angle when a droplet of 5M  $\text{H}_2\text{SO}_4$  is in contact with the surface of as-prepared nanostructured lead. A contact angle of about  $100^\circ \pm 2.3$  indicates that the surface is scarcely wetted by sulfuric acid solution. Therefore, we can conclude that only the top of the nanowires initially works. After 50 cycles contact angle was about  $86^\circ \pm 2.6$  (Figure 8b), while after 200 cycles was not measurable. Likely, initial hydrophobicity of the nanostructures diminishes over cycling owing to the repeated conversion reactions  $\text{Pb}/\text{PbSO}_4$  and vice-versa, which modify the external surface of the nanostructures. Thus, the improvement of the performances is due to the gradual increase of the wetted surface by the electrolyte, therefore polarization decreases. In addition, the modification of the nanowire surface area, due to the conversion reactions  $\text{Pb}/\text{PbSO}_4$  and vice-versa is coupled to porosity increase of the active area, as evident in Figure 9 showing the SEM images of lead electrode cycled at 10C for 200 cycles at the end of charge. This image clearly displays that the morphology of the electrode is quite different in comparison with the as-prepared electrode shown in Figure 3. Obviously, the morphology change is likely due to the continuous volume variation during the conversion reaction of  $\text{Pb}$  to  $\text{PbSO}_4$  and vice-versa. Figure 9 shows that the initial nanowires were changing in micropillars, with very different length, but still well attached to the substrate. Besides, it can be seen that a free space separates neighbouring micropillars. This morphological variation leads to an active material that has both a high surface area, vital for the electrochemical reactions, and a high degree of porosity, which facilitates transport of the electrolyte throughout active material. Similar conclusions were found also by Chen et al, in the case of galvanostatic oxidation of pure  $\text{Pb}$  [70].

The change of electrode morphology was also investigated at the end of the discharge, when the active material was converted in lead sulphate. Figure 10 shows SEM pictures of nanostructured electrodes cycled at 1C for 450 cycles (a and b) and 10C for 1500 cycles (c and d), both at the end of discharge. Obviously, the pillar morphology of the as-prepared electrode is completely lost owing to the conversion in lead sulphate in the form of macroparticles. In particular, these SEM images show that the particle size after 10C cycling

is lower than after 1C, according to the literature showing that as the cycling rate increases, i.e. the current density increases, the mean particle size decreases [71, 72]. Since the magnification of the images is identical, the particles number per surface unit after cycling at 1C is less than after 10C. Therefore, the surface is more porous in this last case. This conclusion is further confirmed by the images of Figure 11, where morphologies of lead electrodes after 50 cycles at 1C (Figure 11a) and 10C (Figure 11b) are shown, both at the end of discharge. This Figure evidences that after 50 cycles smaller particles were formed at 10C than 1C. Therefore, according to the previous considerations, a more porous layer is formed at 10C than 1C also at low cycle number.

According to these results, we can infer that the change of morphology with the consequent gradual increase of both wettability and porosity over cycling is the most likely cause of the better performances of lead nanostructured electrode in comparison with the pasted one.”

While at pag.12 in the conclusions section we have inserted the following sentence: “enough to gain a reliable picture of the electrode performance. The behaviour of nanostructured lead as a negative electrode of an electrochemical cell simulating a LAB found in the present work is potentially of technological interest in comparison with behaviour of the pasted lead electrode, usually employed in current commercial LABs. A likely cause of the better behaviour of the nanostructured lead has been attributed to a combined action of wettability and porosity enhancement over cycling.”



# **Template Electrodeposition and Characterization of Nanostructured Pb as a Negative Electrode for Lead-Acid Battery**

Maria Grazia Insinga, Roberto Luigi Oliveri, Carmelo Sunseri, Rosalinda Inguanta

Laboratorio di Chimica Fisica Applicata, Dipartimento dell'Innovazione Industriale e Digitale-  
Ingegneria Chimica Gestionale Informatica Meccanica, Università di Palermo, Viale delle Scienze,  
90128 Palermo, Italy

## **Highlights**

- Nanostructured lead is checked as a negative electrode for new lead acid battery
- Initial porous structure formed by interconnected nanowires disappears under cycling
- Very high performance was obtained for at 10 C-rate.
- Performances progressively improve reaching cycling efficiency of 100%
- Good stability up to 1500 cycles without fading was observed.

# Template Electrodeposition and Characterization of Nanostructured Pb as a Negative Electrode for Lead-Acid Battery

Maria Grazia Insinga, Roberto Luigi Oliveri, Carmelo Sunseri, Rosalinda Inguanta\*

Laboratorio di Chimica Fisica Applicata, Dipartimento di Ingegneria dell’Innovazione Industriale e Digitale-Ingegneria Chimica Gestionale Informatica Meccanica, Università di Palermo, Viale delle Scienze, 90128 Palermo, Italy

## Abstract

Despite Lead Acid Battery (LAB) is the oldest electrochemical energy storage system, diffusion in the emerging sectors of technological interest is inhibited by its drawbacks. The principal ones are low energy density and negative plate sulphating on high rate discharging. In this work, it is shown the possibility of overcoming such drawbacks by using nanostructured lead as a negative electrode. Lead nanowires (NWs) were fabricated by electrochemical deposition in template, which is an easy, cheap, and easily scalable process. Their morphology and crystal structure have been characterized by electron microscopy and X-ray diffraction, respectively. An electrochemical cell simulating LAB has been assembled with PbO<sub>2</sub> as a counter electrode and an AGM separator, both from commercial battery. Cycling tests were conducted at 10C-rate, setting the cut-off voltage on discharging at 1.2 V. For comparison, also cycling tests at 1C-rate have been carried out, in otherwise identical conditions. At both C-rates, performances in terms of cycling efficiency and lifetime were found a lot better than those of current LABs. The high porosity formed under cycling at 10C-rate provides a reliable explanation of the results.

## Keywords

Lead nanowires, template electrodeposition, lead-acid battery, nanostructures, cycling efficiency, high C-rate cycling.

---

\* Corresponding author:  
[rosalinda.inguanta@unipa.it](mailto:rosalinda.inguanta@unipa.it) (Rosalinda Inguanta)

## 1.0 Introduction

Currently, lead-acid batteries (LABs) are extensively used because are cheap, safe, and almost completely recyclable [1-5]. An interesting study on lead recovery from spent battery was recently authored by Tanong et al. [6] who dealt with the challenging problem concerning metal recovery from a mixture of spent batteries, differently from the current recycling processes that are mainly applied to treat each type of spent battery separately. Over 80% energy efficiency and low self-discharge are additional features that support the wide spread of LABs in the global battery market [7], even if Li-ion battery was replacing such a dominant position [8]. Another strong advantage of LABs is the simple fabrication technology that is well established after more than a century of investigation and continuous improvement [9]. Currently, LABs are largely preferred for applications such as starting lighting ignition (SLI), and stationary storage systems such as uninterruptible power supply (UPS) [10-14]. Low specific energy, poor cyclability in partial state of charge owing to hard sulfation of the negative plates and insufficient active material utilizations (30% of positive plate materials at 1C-rate) [15, 16], are weak features of the LABs. Therefore, they are excluded from those emerging applications requiring heavy deep cycling such as electric vehicle, grid load levelling, telecommunication systems, and so on. Repeated deep discharge and/or high rate partial state of charge operations shorten the lifetime owing to “hard sulfation” of the active materials, in particular of the negative plate. Consequently, extensive investigations are in progress for improving operating performances at high rate state of charge by addition of carbonaceous materials to negative paste [17, 18].

Therefore, huge research efforts are made to do LABs suitable for growing applications such as sustainable mobility, i.e. a transport system exclusively oriented to decarbonisation [19, 20]. For powering either Hybrid or Full Electric Vehicles (EVs), which are largely preferred in the future transport scenarios, the huge battery requirement, in addition to high specific energy, is long lifetime under continuously cycling at high rate in the partial state of charge (HRPSoC) owing to the intermittent operation of the EVs. Such a requirement is today full satisfied by Li-ion batteries, which are unsafe and, currently, highly expensive [21]. The subject matter dealing with the lead-acid battery performance at HRPSoC has been extensively investigated and different solutions were proposed such as modifying the negative active material composition through suitable additives, designing innovative assembly with super-capacitor, or improving the energy efficiency through proper managing of the charging process [22-26].

The performance limits of the LABs originate from their design [27, 28]. Currently, a plate is formed by porous paste and lead grid pressed together, where the paste acts as an active material and grid as a current collector. The plates are vertically arranged with consequent sulphuric acid



1 stratification that favours hard sulfation, particularly at high C-rate [29, 30]. In addition, the contact  
2 between grid and active material is critical owing to possible electrical conduction interruption due  
3 to insulating lead sulphate formation on discharging and grid corrosion of positive plate [31]. For  
4 applications where high C-rates are requested, the thickness must be as low as possible, because the  
5 volume expansion of both positive and negative plates occurring on discharging causes the partial  
6 pore occlusion with consequent loss of the electrolyte continuity between the external and interior  
7 part of the plate. In practice, lead dioxide at the positive plate and metallic lead at the negative plate  
8 form lead sulphate on discharging with concomitant volume increase of 92% and 164%,  
9 respectively [32].

10  
11 Almost all these drawbacks might be overcome by changing the morphology of the active  
12 materials. In particular, the nanostructures synthesis method developed in our lab, and described in  
13 [33-38] has been proved to be extremely effective. Our previous works revealed significant  
14 improvements in the charge/discharge performances of  $\text{PbO}_2$  nanowires (NWs) synthesized through  
15 this method [39-42]. The same technique has been extended to Pb electrode for fabricating negative  
16 electrode of a possible innovative LAB having both anode and cathode with nanostructured  
17 morphology. Preliminary results [43, 44] showed that it is possible to deposit compact lead NWs  
18 from aqueous solution avoiding dendrite formation. This was the major challenge investigated for  
19 long time, so that formation of Pb nanostructures was also proposed through electrochemical  
20 reduction of  $\text{PbO}_2$  NWs [45] because their electrodeposition in template was found to be a lot easier  
21 [46]. This way was discarded being direct deposition of lead nanostructures more useful from a  
22 technological point of view because i) electrode fabrication process is simpler, and ii) NW shape is  
23 more regular so guaranteeing a better mechanical stability under cycling when repeated volume  
24 expansion and contraction occur. In fact, Pb NWs from  $\text{PbO}_2$  electrochemical reduction show a  
25 typical wave-like shape due to the density reduction accompanying the conversion of the oxide to  
26 metallic lead. The mechanical stability of the NWs is of primary importance for drawing the  
27 expected advantages of the nanostructured morphology, primarily consisting in a very low active  
28 material thickness.

29  
30 In comparison with positive plates, the negative ones suffer from specific problems such as  
31 easier hard sulfation and tendency of the metallic lead to form dendritic structures on conversion  
32 from lead sulphate [47]. The formation of dendrites is undesired because can puncture the separator  
33 with consequent cell out of service due to anode/cathode short circuit. For improving the negative  
34 plate performances at high C-rate, either addition of various materials to the active paste [48-55] or  
35 use of modified grids [56-59] have been investigated in the past.

The idea inspiring the present work was the use of a nanostructured lead electrode to improve the performance of lead-acid battery at a level that cannot be achieved through the pasted materials. After preliminary investigations aimed essentially to check the viability of depositing nanostructured lead in one step [44], here, we present the results of a systematic study on both the synthesis of a lead nanostructured array and its use as a negative electrode in a lab cell simulating a lead acid battery. For the first time, at our best knowledge, results are presented dealing with a lead electrode cycled for more than 1500 times at 10C-rate in 5M H<sub>2</sub>SO<sub>4</sub> without fading. Besides, a correlation between charge/discharge performance and morphology is established, with the help of a strict comparison of the behaviour of electrodes cycled at 1C-rate in otherwise identical conditions.

## 2.0 Materials and Methods

### 2.1 Electrode fabrication

The nanostructure fabrication was carried out according to the method proposed elsewhere [33]. In particular, a Whatman polycarbonate membrane was used as a template. For making it electrically conductive, a 20-30 nm thick gold film was sputtered on one side. The principal advantages in using a polycarbonate membrane are i) easy removal by chemical dissolution in dichloromethane without damaging the nanostructures, and ii) successive recovery of the polycarbonate by batch distillation.

A compact layer of lead was electrochemically deposited on the gold film for the dual purpose of i) supporting the nanostructures, and ii) connecting electrically them to the power supply. It was selected to support NWs through an identical material to inhibit self-discharge effects. The Pb layer growth was highly challenging because lead electrochemical deposit tends to be fibrous in texture and possesses a degree of porosity [60]. For avoiding the formation of such a structure, a proper composition of the tetrafluoboric-based solution was developed containing 4.5g L<sup>-1</sup> lignin sulfonate (C<sub>20</sub>H<sub>26</sub>O<sub>10</sub>S<sub>2</sub>), 15g L<sup>-1</sup> H<sub>3</sub>BO<sub>3</sub>, 35.2g L<sup>-1</sup> HBF<sub>4</sub>, and 40.5g L<sup>-1</sup> Pb(BF<sub>4</sub>)<sub>2</sub>. The cell was assembled with a Pt mesh as a counter electrode, and powered by a pulsed rectangular current (duty cycle = 0.952) supplied by a PAR Potentiostat/Galvanostat (mod. PARSTAT 2273). Deposition was conducted in three identical steps of 960 s each. At the end of every step, the solution was replaced with a fresh one, for avoiding any relevant modification of the precursor concentration favouring acicular morphology formation. The shape of the rectangular current pulse is shown in Figure 1, where it is also evidenced the cell voltage response. After preliminary investigations leading to a 30 μm thick compact Pb layer, the design of the cell was improved so that now, it is possible to grow a half thinner layer without damaging the mechanical stability of the

overlying nanostructures. Thinning the lead layer is a relevant result because decreases the inert mass, i.e. the mass not involved in battery operation.

Deposition of the lead nanostructures was conducted in almost identical conditions of the layer underlying the nanostructures. In particular, nature and composition of the precursor solution were identical and the current pulse shape was rectangular with a duty cycle of 0.91. Figure 2 shows some current pulses together with the voltage response. Also in this case, a Pt mesh was used as a counter electrode, and a pulsed rectangular current supplied by a PAR Potentiostat/Galvanostat (mod PARSTAT 2273) powered the cell. NWs growth was carried out in a 450 s long single step, and a nanostructure was obtained about 10  $\mu\text{m}$  thick.

The nanostructures were characterized at the end of their synthesis and after chemical dissolution of the template in order to fully expose their structure. This operation must be conducted with care for avoiding collapse of the deposited Pb NWs with consequent discarding of the electrode. The template dissolution was carried out in successive steps for its complete removal as proposed in [33, 61].

A Field Emission Gun Environmental Scanning Electron Microscope (FEI Quanta 200 FEG-ESEM) was employed for morphological analysis while solid-state characterization was performed through a RIGAKU X-ray diffractometer (model: D-MAX 25600 HK). X-ray diffraction patterns were obtained in the  $2\theta$  range from  $10^\circ$  to  $100^\circ$  with a sampling width of  $0.004^\circ$  and a scan speed of 3 deg./min, using Ni-filtered Cu  $K\alpha$  radiation ( $\lambda = 1.54 \text{ \AA}$ ). Diffraction peaks were identified by comparison with ICDD database (International Centre for Diffraction Data 2007). In addition, electrode wettability was evaluated by contact angle measurements using a 5 M sulphuric acid solution as wetting liquid (FTA 1000 First Ten Ångströms). Contact angle was performed on different areas of the nanostructured electrodes to evaluate their uniformity.

## 2.2 Electrode test

The nanostructured lead was tested as a negative electrode in an electrochemical cell simulating a LAB, where pasted  $\text{PbO}_2$  from commercial battery acted as a positive electrode. The two electrodes were vertically assembled, isolated by an AGM separator from a commercial battery, and immersed in 5M  $\text{H}_2\text{SO}_4$ . A zero-gap cell, held at  $25 \pm 2^\circ\text{C}$ , was assembled to exclude any effect on the electrochemical results of both cell configuration and uncontrolled temperature oscillations. The cell was powered at constant current through a Cell Test System (Solartron, Mod. 1470 E, 8 channels) controlled by a desk computer via MultiStat Software (Mod. UBS147010ES). The voltage value reported in the following is the difference in electric potential between positive ( $\text{PbO}_2$ ) and negative (Pb) electrodes. It was not used any reference electrode in order to compare the

cell voltage value directly with a real LAB, whose performances and the State of Charge are evidenced just through the cell voltage.

The nominal charge capacity of the negative electrode was determined by weight according to the following steps.

- 1) After sputtering of the gold film, the membrane was weighed, up to a constant weight;
- 2) Then, the Pb layer acting as a support for the nanowires and current collector was deposited on the gold film. The membrane was again and again weighed up to a constant weight;
- 3) Then, nanowires were electrochemically deposited inside the membrane channels and weight of the membrane was determined after repeated measurements to a constant value;
- 4) The weight difference prior to and after nanowires deposition gave the nanowire mass deposited;
- 5) According to the reaction stoichiometry, one mole of Pb is equivalent to 53.6 Ah of electrical charge. Therefore, the electrical capacity of the nanostructured Pb electrode was determined within a span error of  $\pm 5\%$ , which was considered as highly satisfying.

Only the weight of the NWs was considered in evaluating the nominal capacity, because dedicated experiments showed that the Pb layer supporting the NWs does not participate to the battery cycling. The weight determinations were operated by a SARTORIUS microbalance (mod.: ME36S Premium Microbalance). More than 100 times higher electrical capacity of PbO<sub>2</sub> counter-electrode was selected, so that the nanostructured electrode was controlling the cell performance.

The electrochemical tests were conducted at constant current corresponding to 10C-rate. For better evaluating the performances of lead NWs, also tests at 1C-rate were conducted. The charging stage was conducted by limiting the voltage to 2.85 V, because a cell reaching higher voltages was considered as permanently damaged (with the exception of the first charging). Besides, charge acceptance was evaluated by limiting charging duration at either 6 mins (10C-rate) or 60 mins (1C-rate). Of course, some electrical charge is lost for hydrogen evolution in dependence on the voltage. Such an uncertainty has to be accepted if a simulation close to the real operation is desired. In real conditions, hydrogen is evolved during charging at more or less extent in dependence on the state of the negative electrode. In practice, cell voltage, whose value determines water-splitting extent, is a valuable function cell indicator.

In the present study, the function test concerns exclusively the negative electrode because the cell was assembled in such a manner to ensure the cycling control by the nanostructured electrode. For this reason, the cell voltage on charging was limited at prefixed values, above which the electrode was discarded.

The first charging was conducted differently, as the C-rate was stepwise grown from 0.2C-rate to 10C-rate. This charging procedure was successfully experienced previously [40, 44], and here was extended to rate higher than 1C-rate.

Discharge stage was conducted at the same C-rate of the charging. Two limits were imposed consisting in cut-off cell voltage and discharging time length. The first one was set at 1.2 V in order to check the lifetime of the nanostructured negative electrode under such a stressing condition that determines rapid sulfation of the commercial LABs. The duration of discharging was limited to drawing 90% of the nominal capacity; therefore, the time was set at 5.4 and 54 min for 10C and 1C-rate, respectively. Such a 90% limit was selected for avoiding of converting all available lead into insulating sulphate, with consequent voltage spike above 2.85 V on the starting of the successive charging.

The double limit on discharging gives a more complete picture of the performance of the electrode under study. In fact, if the electrode polarizes to the cut-off voltage within the selected time, discharging stops and a new charging starts. On the contrary, if the electrode polarization remains for all the selected duration less than the cut-off voltage, then the process inverts at time compliance. In this case, it can be assumed that 90% of the accepted charge is drawn; therefore a cycling efficiency of 100% has to be estimated, as ratio of the drained charge to the accepted one.

### 3.0 Results and Discussion

Lead layer deposition on the gold film was conducted prior to fabricating the nanostructured negative electrode. Figure 1 shows the rectangular current pulses powering the electrochemical cell together with the voltage response, which was changing with the advancement of the deposition process, as shown by comparing Figure 1a, b, and c. It can be observed that the voltage remains constant at about -2.25 V during the first stage of deposition, while shows an increasing trend to -2.19 V during the successive two steps. Since oxygen evolution is the reaction always occurring at the counter electrode that remains unchanged, the observed voltage variation during the current pulses have to be attributed to modification in the deposition process of lead. Really, during the first stage, lead is deposited on gold, whose coverage is complete likely at the end of this stage. In the successive stages, deposition of lead on lead occurs. This interpretation is supported by the slight higher voltage during the first stage (-2.5 V) because the deposition of lead on gold is kinetically more difficult than deposition of lead on lead where there is not crystal lattice mismatching. The increasing trend of the voltage in Figure 1b and 1c can be attributed to the onset of concentration polarization which is removed during the current inversion. This trend justifies why duration of each deposition stage was limited at 960 sec. The renewal of the solution, after each step, was due

to eliminate any risk of dendrite or acicular deposit formation that are favoured by decreasing lead concentration [62].

On the contrary, lead deposition inside the template was carried out in 450 s long single step, sufficient to deposit about 10  $\mu\text{m}$  high NWs. Figure 2 a shows some current rectangular pulses and the consequent cell voltage response that is slowly sloping during each constant cathodic current interval. Here, the prevalent polarization occurs in the initial instants of the cathodic pulse, likely due to combined effects of ohmic drop and concentration overpotential in a confined ambient such as nanosized template channels. Also in this case the concentration overpotential was removed on the current inversion.

The typical morphology of the as-prepared lead nanostructures is shown in Figures 2 b-d. Porosity generated by uniform distribution of NWs is clearly visible in Figures 2 b and c. The NW interconnection is conformal to the template morphology. The section view of Figure 2 d shows the firm connection of NWs to the support, and the void space useful for accommodating the volume increase on discharging.

Typical crystal structure of the lead electrode is shown in Figure 3, where XRD patterns of the as-prepared (Figure 3a) and cycled electrode up to end of life (Figure 3b) are shown. In Figure 3a, very strong lead peaks are evident together with some weak peaks attributed to more or less hydrated  $\beta\text{-PbO}$ , likely formed on air exposition of the as-prepared Pb NWs. In practice, XRD analysis reveals the extreme purity of the as-prepared deposit. For the sake of comparison, the typical XRD pattern of an electrode disassembled after cycling in 5M  $\text{H}_2\text{SO}_4$  up to end of life is shown in Figure 3b. Strong  $\text{PbSO}_4$  peaks are largely present together with some weaker peaks of lead, which might be attributed to either residual lead or to the underlying layer supporting the nanostructures. The XRD pattern at the end of life is independent of the cycling C-rate.

The performance tests of the nanostructured lead as a negative electrode of a simulated LAB was conducted at 10C-rate (Figure 4). For comparison, tests at 1C-rate were also carried out in order to establish the influence of the cycling rate on the lifetime (Figure 5). In addition, tests were conducted at as a low cut-off voltage as 1.2 V. High C-rate and deep depth of discharge were selected for severely stressing the electrode in comparison with LAB pasted one, which cannot sustain such conditions without fast sulfation [63]. Testing initial stage was the stepwise charging of the as-prepared nanostructured electrode, followed by discharging conducted at the same rate of the last charging step. Then, the electrode was cycled at the selected C-rate. Figures 4a and 5a show both the initial step-by-step charge up to 10C and 1C, respectively. The stepwise implement of the C-rate for charging the as-prepared lead NWs was found extremely effective for maintaining the cell voltage below 3.0 V, so preserving the active material from any damage due to turbulent gas

1 evolution. The first discharging curve shows a fast polarization of the electrode, likely due to the  
2 high reactivity of the NWs, which convert in sulphate almost instantaneously. In practice, the first  
3 discharge does not deliver any useful electrical charge at both 10C and 1C-rate. The higher voltage  
4 drop on reversing the first charging shown in Figure 4a in comparison with Figure 5a has to be  
5 attributed to the higher current at 10C than 1C-rate. Of course, at 10C-rate the conversion of Pb to  
6 PbSO<sub>4</sub> is ten times faster and, consequently the ohmic drop is higher. As reported below, a role can  
7 be also attributed to the wettability of the porous mass, because the wettability of solid  
8 nanostructure and its permeation by a liquid solution is an important aspect for the behaviour of  
9 nanostructured materials, as recently shown [64, 65]. In this context, Moncada et al. [40] evidenced  
10 a specific influence of the wettability on the performance of nanostructured PbO<sub>2</sub> acting as a  
11 positive electrode.  
12

13 On cycling after the stepwise initial charging, the delivered charge always increases  
14 independently of the C-rate. Figures 4b and 4c show the cycling curves at 10C-rate of lead NW  
15 electrode (5b), and the related faradic efficiency (4c). Figure 5b evidences a strong polarization on  
16 charging of the electrode at cycle #10 (curve a), where a voltage of 2.8 V close to the limiting value  
17 of 2.85 V is reached. The polarization decreases with the cycling as shown by the curve b (50<sup>th</sup>  
18 cycle) featured by an initial low polarization interval followed by an inflection at about 6 mAh g<sup>-1</sup>  
19 leading to a quasi steady-state voltage of about 2.7 V. It is interesting to observe that the low  
20 polarization interval length increases with the cycling number up to a value of 11.5 mAh g<sup>-1</sup> at the  
21 1500<sup>th</sup> cycle (curve f). Besides, also the quasi steady-state voltage following the inflection is  
22 decreasing to 2.5V over charging. The two levels of polarization can be explained taking into  
23 account the reactions occurring on charging. Neglecting the reduction of the dissolved oxygen  
24 owing to its saturation concentration which is as low as 0.61 mM in 5.4M H<sub>2</sub>SO<sub>4</sub> [66], the reactions  
25 that have to be considered are PbSO<sub>4</sub> conversion into Pb, and hydrogen evolution. Initially, the  
26 prevailing process is the reduction of PbSO<sub>4</sub> to Pb, because it occurs at lower overvoltage [67] than  
27 hydrogen evolution on lead [68]. As the PbSO<sub>4</sub> conversion into Pb is almost complete, the  
28 prevailing reaction becomes hydrogen evolution, which occurs with higher overvoltage. In practice,  
29 the applied current of charging is divided up into PbSO<sub>4</sub> and H<sub>3</sub>O<sup>+</sup> reduction. In the initial stage, the  
30 partial current of PbSO<sub>4</sub> conversion is prevailing and a low voltage is found. When the partial  
31 current of hydrogen evolution becomes prevalent higher voltage is recorded even if the conversion  
32 of PbSO<sub>4</sub> continues but at lower partial current. The curve inflection marks the transition from one  
33 regime to the other one. This is a typical voltage response of a lead-acid cell at constant rate charge  
34 [69].  
35  
36  
37  
38  
39  
40  
41  
42  
43  
44  
45  
46  
47  
48  
49  
50  
51  
52  
53  
54  
55  
56  
57  
58  
59  
60  
61  
62  
63  
64  
65

The increasing extension of the charging interval prior to the inflection finds its explanation in the discharging curves. Moving from curve a' (10<sup>th</sup> cycle) towards those relative at higher cycle number, not only the drained charge increases but also the discharging process runs with lower overvoltage. In particular, curves c' (100<sup>th</sup> cycle) and d' (500<sup>th</sup> cycle), show an almost rectangular shape matching the theoretical one. Besides, it must be observed that the discharging process is controlled still by cut-off voltage at the 500<sup>th</sup> cycle, while time length is controlling at the 1000<sup>th</sup> cycle and successive (curves e', and f' of Figure 4b whose shape will be explained below in the light of Figure 8). Therefore, the low voltage interval over charging extends progressively because the drained charge is progressively increasing. As discharging process passes from cut-off voltage to the time control, then, it can be assumed that the total nominal capacity is drained, otherwise the electrode should have been polarized owing to the formation of insulating PbSO<sub>4</sub>. This means that the charge/discharge process runs with 100% faradic efficiency, therefore, its curve has to be normalised at 100% like in Figure 5c. This plot is coherent with the findings of Figure 4b, because it shows a progressive increase of the efficiency with the number of cycles. Therefore, the LAB under investigation improves its performance on cycling to the point that it works after 1500 cycles without fading. At our best knowledge, such behaviour of a LAB negative electrode has been found and reported here for the first time. This result is of great relevance in comparison with the pasted negative electrodes of the commercial batteries, which cannot sustain these severe cycling conditions, without undergoing to fast sulfation.

Another advantage of the nanostructured negative electrode is shown in Figure 5b, where the curves over cycling at 1C-rate are reported. It can be observed that also in this case, the performances improve under cycling, with the big difference that the electrode polarization is greater at 1C than 10C-rate. In particular, the curve f'(450<sup>th</sup>) shows that the highest charge is drained with the highest overvoltage essentially due to the initial voltage spike. Such sharp drop can be attributed likely to the presence of sulphate that has not converted during the previous stage of charging. Therefore, when LAB is cycled at 1C-rate its lifetime is shorter because hard sulphate is present already at 450<sup>th</sup> cycle in such a quantity to determining high cell polarisation, differently from the nanostructured lead electrode that works up to 1500 cycles at 10C-rate without any difficulty. The cycling at 10C-rate was stopped at 1500<sup>th</sup> cycle only for the sake of characterizing the electrode after so long time of immersion (12.5 days); otherwise the cell could continue to cycling. It was estimated that 1500 cycles at 10C-rate without fading had to be considered a so very satisfying result that did not need to prolong the cycling.

Figure 5c shows a typical plot of cycling efficiency at 1C-rate vs cycles. The efficiency curve is consistent with the cycling curves of Figure 5b, because it is evidenced that the efficiency



not only never reaches the value of 100%, but remains almost constant at around 90% from about 280<sup>th</sup> cycle to the 450<sup>th</sup>. Figures 4 and 5 clearly indicate that when electrodeposited nanostructured lead is employed as a negative electrode in a cell simulating a LAB, not only electrode polarization decreases but also efficiency improves under cycling and with C-rate. These findings are different in comparison with the behaviour of current commercial LABs pasted electrodes which decay rapidly if cycled under the stressing conditions selected for testing nanostructured electrodes. In this context, it is mandatory to scrutinize the possible causes of such behaviour.

At this aim, dedicated investigations were conducted. First of all, the wettability of the nanostructured electrode was determined. Figure 6a shows the contact angle when a droplet of 5M H<sub>2</sub>SO<sub>4</sub> is in contact with the surface of as-prepared nanostructured lead. A contact angle of about 100°±2.3 indicates that the surface is scarcely wetted by sulfuric acid solution. Therefore, we can conclude that only the top of the nanowires initially works. After 50 cycles contact angle was about 86°±2.6 (Figure 6b), while after 200 cycles was not measurable. Likely, initial hydrophobicity of the nanostructures diminishes over cycling owing to the repeated conversion reactions Pb/PbSO<sub>4</sub> and vice-versa, which modify the external surface of the nanostructures. Thus, the improvement of the performances is due to the gradual increase of the wetted surface by the electrolyte, therefore polarization decreases. In addition, the modification of the nanowire surface area, due to the conversion reactions Pb/PbSO<sub>4</sub> and vice-versa is coupled to porosity increase of the active area, as evident in Figure 7 showing the SEM images of lead electrode cycled at 10C for 200 cycles at the end of charge. This image clearly displays that the morphology of the electrode is quite different in comparison with the as-prepared electrode shown in Figures 2 b-c. Obviously, the morphology change is likely due to the continuous volume variation during the conversion reaction of Pb to PbSO<sub>4</sub> and vice-versa. Figure 7 shows that the initial nanowires were changing in micropillars, with very different length, but still well attached to the substrate. Besides, it can be seen that a free space separates neighbouring micropillars. This morphological variation leads to an active material that has both a high surface area, vital for the electrochemical reactions, and a high degree of porosity, which facilitates transport of the electrolyte throughout active material. Similar conclusions were found also by Chen et al, in the case of galvanostatic oxidation of pure Pb [70].

The change of electrode morphology was also investigated at the end of the discharge, when the active material was converted in lead sulphate. Figure 8 shows SEM pictures of nanostructured electrodes cycled at 1C for 450 cycles (a), 10C for 1500 cycles (b) and after 50 cycles at 1C (c) and 10C (d). All images were made at the end of discharge. Obviously, the pillar morphology of the as-prepared electrode is completely lost owing to the conversion in lead sulphate in the form of macroparticles. In particular, these SEM images show that the particle size after 10C cycling is

lower than after 1C, according to the literature showing that as the cycling rate increases, i.e. the current density increases, the mean particle size decreases [71, 72]. Since the magnification of the images is identical, the particles number per surface unit after cycling at 1C is less than after 10C. Therefore, the surface is more porous in this last case. This conclusion is further confirmed by the images after 50 cycles at 1C (Figure 8 c) and 10C (Figure 8 d) are shown, both at the end of discharge. This Figure evidences that after 50 cycles smaller particles were formed at 10C than 1C. Therefore, according to the previous considerations, a more porous layer is formed at 10C than 1C also at low cycle number.

According to these results, we can infer that the change of morphology with the consequent gradual increase of both wettability and porosity over cycling is the most likely cause of the better performances of lead nanostructured electrode in comparison with the pasted one.

In detail, fresh formed nanostructured lead shows the pillar morphology of Figure 2 b-d. Over cycling, conversion reaction of lead sulphate to lead and vice-versa occurs ~~during charging and discharging, respectively~~, therefore, the initial morphology is progressively lost, as shown in Figure 7. Figures 4a, and 5a show that the first discharge is so fast that no electrical charge is drained, because, likely, ~~the scarce wettability of the nanostructured electrode so that only the top of the nanowire is completely~~ converted into lead sulphate with immediate polarization to the cut-off voltage. As cycling is continued, the drained charge progressively increases, as shown in Figures 4b and 5b ~~because both wettability and porosity increase. These results support the conclusion that, on cycling, the NWs converts into particles uniformly distributed on the compact lead layer so to create a porosity that could not be generated with any other method, thus confirming that the porosity improvement with C-rate may be attributed to the rate at which the conversion reactions occur. In the light of Figure 8, it is possible to explain also the shape of curve e' and f' of Figure 6a. As detailed above, the electrode performances improves with both C-rate and cycle number, owing to morphology change under cycling. Starting from the initial nanowire array, the porosity progressively increases for identical geometrical surface due to conversion reactions from Pb to PbSO<sub>4</sub> and vice-versa.~~ The enhancement of the reacting area determines a decrease of the electrode polarization with a consequent increase of the drained charge on discharging, as clearly shown in Figure 4b and 5b. The depolarization of the electrode processes is more effective at 10C than 1C in otherwise identical conditions, because, at higher C-rate the particle size decreases and porosity increases more. Therefore, at 10C, the cell voltage does not reach the cut-off value (1.2V) during 324 sec (= 0.9\*360) long discharge. For this reason, the curves e', and f' of Figure 4b are so slowly sloping to seem almost flat, in contrast with the usual shape of discharging curves of a battery.

More work is in progress to detect the highest C-rate leading to significant improvement of performances. Cycling of lead NWs seems to have the same effect of the curing in the fabrication of the commercial plates. The comparison is only general, because the processes occurring in the two cases are completely different as different is the usability of the battery. The only similitude is the final effect, because both processes develop the active material porosity, which controls operative performances of the battery.

## Conclusions

Nanostructured lead electrode, fabricated through electrochemical deposition in template, shows amazing performances when used as a negative electrode in an electrochemical cell simulating a LAB. The innovative finding presented and discussed in the present work is the behaviour of such an electrode under cycling in highly stressing conditions. Indeed, the lab cell was cycled at 10C-rate for 1500 cycles with a cut off voltage of 1.2V on discharging. Such conditions favour fast hard sulphation of the pasted LAB electrodes. On the contrary, nanostructured electrode not only sustains these conditions for high cycle number, but also progressively improves its performances reaching cycling efficiency of 100% up to 1500 cycles without fading. The cycling was stopped at the 1500<sup>th</sup> cycle only for the sake of characterization, since 12.5 days of cycling were considered enough to gain a reliable picture of the electrode performance. The behaviour of nanostructured lead as a negative electrode of an electrochemical cell simulating a LAB found in the present work is potentially of technological interest in comparison with behaviour of the pasted lead electrode, usually employed in current commercial LABs. A likely cause of the better behaviour of the nanostructured lead has been attributed to a combined action of wettability and porosity enhancement over cycling.

Such valuable finding has been explained in terms of modification of the electrode wettability and porosity under cycling. In addition, ~~it has been shown that the porosity modification is strongly dependent on the C-rate, so that~~ the better performances were found at 10C than 1C, therefore the drained capacity decreasing over cycling, typical of commercial LAB, is no longer true when a nanostructured electrode is used. ~~The original nanostructured morphology of the lead negative electrode (lead nanowires) favours the progressive improvement of the electrode performance likely due to development under cycling of a porosity which cannot be obtained with any other method. This finding is even more significant taking into account the high C-rate (10C).~~

In practice, nanostructured lead could be a valuable electrode for innovative LAB because it works very well where negative plate of commercial LAB fails. Since also nanostructured PbO<sub>2</sub> can

sustain 10C-rate for long cycling, experimental LABs with both nanostructured electrodes are under investigation.

No less interesting are the results of the present work concerning the nanostructure fabrication process, which is easy to be conducted, cheap, and easily scalable. In addition, the polycarbonate, which is the material of the template, can be easily recovered and recycled. Identically, dichloromethane, which is the chemical for dissolving the template at the end of the nanostructure fabrication, can be recovered with high purity.

Therefore, the challenge can be accepted for trying construction of a LAB prototype with both nanostructured electrode after having addressed other issues such as self-discharge, temperature profile on discharging, performance at high and low temperatures, and more favourable weight ratio of porous mass to support layer acting also as a current collector.

## Acknowledgements

This work was supported by Europe Union and co-funded by Italian Ministry of Education [grant PON03PE\_00214\_1 “Nanotecnologie e nanomateriali per i beni culturali (TECLA)”]

## References

- [1] X. Tian, Y. Wu, P. Hou, S. Liang, S. Qu, M. Xu, T. Zuo, Environmental impact and economic assessment of secondary lead production: Comparison of main spent lead-acid battery recycling processes in China, *J. Cleaner Production* 144 (2017) 142-148. DOI:10.1016/j.jclepro.2016.12.171
- [2] Z. Sun, H. Cao, X. Zhang, X. Lin, W. Zheng, G. Cao, Y. Sun, Y. Zhang, Spent lead-acid battery recycling in China – A review and sustainable analyses on mass flow of lead, *Waste Manage.* 64 (2017) 190–201, DOI:10.1016/j.wasman.2017.03.007
- [3] A.J. Davidson, S.P. Binks, J. Gediga, Lead industry life cycle studies: environmental impact and life cycle assessment of lead battery and architectural sheet production, *The International J. Life Cycle Assessment*, 21 (2016) 1624–1636. DOI:10.1007/s11367-015-1021-5
- [4] Y. Ma, K. Qiu, Recovery of lead from lead paste in spent lead acid battery by hydrometallurgical desulfurization and vacuum thermal reduction, *Waste Manage.* 40 (2015) 151–156. DOI:10.1016/j.wasman.2015.03.01
- [5] M. Volpe, D. Oliveri, G. Ferrara, M. Salvaggio, S. Piazza, S. Italiano, C. Sunseri, Metallic lead recovery from lead-acid battery paste by urea acetate dissolution and cementation on iron, *Hydrometallurgy* 96 (2009) 123–131. DOI:10.1016/j.hydromet.2008.09.001
- [6] K. Tanong, L. Coudert, G. Mercier, J.-F. Blais, Recovery of metals from a mixture of various spent batteries by a hydrometallurgical process, *J. Environ. Manage.* 181 (2016) 95-107, DOI:10.1016/j.jenvman.2016.05.084
- [7] A. Banerjee, B. Ziv, Y. Shilina, E. Levi, S. Luski, and Doron Aurbach, Single-Wall Carbon Nanotube Doping in Lead-Acid Batteries: A New Horizon, *ACS Applied Materials & Interfaces* 9, 2017, 3634–3643. DOI:10.1021/acsami.6b13377
- [8] Yoshio, M., Brodd, R. J., Kozawa, A., *Lithium-Ion Batteries: Science and Technologies*, Springer, New York, 2009.

- [9] M. Kwiecien, P. Schröer, M. Kuipers, D.U. Sauer, Current research topics for lead–acid batteries in: J. Garche, E. Karden, P.T. Moseley, D.A.J. Rand (Eds.), *Lead-Acid Batteries for Future Automobiles*, Elsevier Inc., Amsterdam, 2017, pp. 133–146. [DOI:10.1016/B978-0-444-63700-0.00004-0](https://doi.org/10.1016/B978-0-444-63700-0.00004-0)
- [10] M. Gelbke, C. Mondoloni, Flooded starting-lighting-ignition (SLI) and enhanced flooded batteries (EFBs): State-of-the-art in: J. Garche, E. Karden, P.T. Moseley, D.A.J. Rand (Eds.), *Lead-Acid Batteries for Future Automobiles*, Elsevier Inc., Amsterdam, 2017, pp. 149–184, [DOI:10.1016/B978-0-444-63700-0.00005-2](https://doi.org/10.1016/B978-0-444-63700-0.00005-2)
- [11] B. Zakeri, S. Syri, F. Wagner, Economics of energy storage in the German Electricity and Reserve Markets, 14th International Conference on the European Energy Market (EEM) Dresden, Germany 6-9 June 2017
- [12] M. Krishna, E.J. Fraser, R.G.A. Wills, , F.C. Walsh, Developments in soluble lead flow batteries and remaining challenges: An illustrated review, *J. Energy Storage* 15 (2018) 69–90. [DOI:10.1016/j.est.2017.10.020](https://doi.org/10.1016/j.est.2017.10.020)
- [13] N. Bashir, H.S. Sardar, M. Nasir, N.U. Hassan, H.A. Khan, Lifetime Maximization of Lead-Acid Batteries in Small Scale UPS and Distributed Generation Systems, 12th IEEE PES PowerTech. Conference Manchester June 18-22 2017.
- [14] R. Wagner, Valve-regulated Lead-Acid Batteries for Telecommunications and UPS Applications in: D.A.J. Rand, J. Garche, P.T. Moseley and C.D. Parker (Eds.) *Valve-Regulated Lead-Acid Batteries*, Elsevier Inc., Amsterdam, 2004, pp. 435–465. [DOI:10.1016/B978-044450746-4/50015-5](https://doi.org/10.1016/B978-044450746-4/50015-5)
- [15] M. Saravanan, M. Ganesan, S. Ambalavanan, An in-situ Generated Carbon as Integrated Conductive Additive for Hierarchical Negative Plate of Lead-Acid Battery, *J. Power Sources* 251 (2014) 20–29. [DOI:10.1016/j.jpowsour.2013.10.143](https://doi.org/10.1016/j.jpowsour.2013.10.143)
- [16] N.Vangapally, S.A. Gaffoor, S.K.Martha, Na<sub>2</sub>EDTA chelating agent as an electrolyte additive for high performance lead-acid batteries, *Electrochim Acta* 258 (2017) 1493-1501. [DOI:10.1016/j.electacta.2017.12.028](https://doi.org/10.1016/j.electacta.2017.12.028)
- [17] M. Saravanan, P. Sennu, M. Ganesan, S. Ambalavanan, Multi-Walled Carbon Nanotubes Percolation Network Enhanced the Performance of Negative Electrode for Lead-Acid Battery, *J. Electrochem. Soc.* 2013, 160, A70–A76. [DOI:10.1149/2.062301jes](https://doi.org/10.1149/2.062301jes)
- [18] W.-L. Zhang, J. Yin, Z.-Q. Lin, J. Shi, C. Wang, D.-B. Liu, Y. Wang, J.-P. Bao, H.-B. Lin, Lead-carbon electrode designed for renewable energy storage with superior performance in partial state of charge operation, *J. Power Sources* 342 (2017) 183-191. [DOI:10.1016/j.jpowsour.2016.12.061](https://doi.org/10.1016/j.jpowsour.2016.12.061)
- [19] J. Zawieska, J. Pieriegud, Smart city as a tool for sustainable mobility and transport decarbonisation, *Transport Policy* 63 (2018) 39-50
- [20] C. Chumchal, D. Kurzweil, Lead–acid battery operation in micro-hybrid and electrified vehicles in: J. Garche, E. Karden, P.T. Moseley, D.A.J. Rand (Eds.), *Lead-Acid Batteries for Future Automobiles*, Elsevier Inc., Amsterdam, 2017, pp. 395-414, [DOI:10.1016/B978-0-444-63700-0.00013-1](https://doi.org/10.1016/B978-0-444-63700-0.00013-1)
- [21] G. Zubi, R. Dufo-López, M. Carvalho, G. Pasaoglu, The lithium-ion battery: State of the art and future perspectives, *Renewable and Sustainable Energy Reviews* 89 (2018) 292–308. [DOI:10.1016/j.rser.2018.03.00](https://doi.org/10.1016/j.rser.2018.03.00)
- [22] M. Fernández, F. Trinidad, J. Valenciano, A. Sánchez, Optimization of the cycle life performance of VRLA batteries, working under high rate, partial state of charge (HRPSOC) conditions, *J. Power Sources* 158 (2006) 1149-1165.
- [23] C. Snyders, E.E. Ferga, T. van Dyl, The use of a Polymat material to reduce the effects of sulphation damage occurring in negative electrodes due to the partial state of charge capacity cycling of lead acid batteries, *J. Power Sources* 200 (2012) 102-107. [DOI:10.1016/j.jpowsour.2011.10.087](https://doi.org/10.1016/j.jpowsour.2011.10.087)

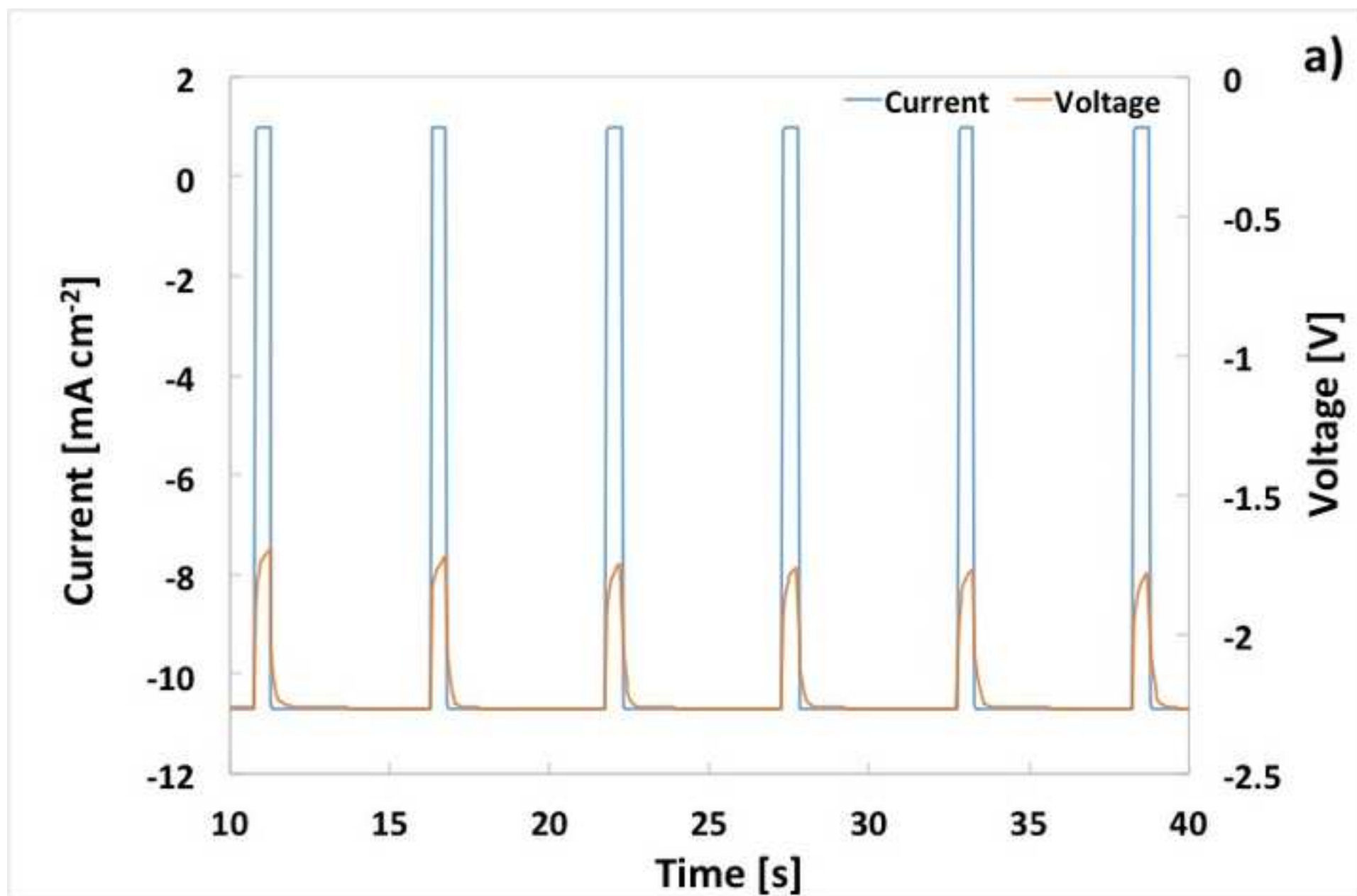
- [24] Banerjee, B. Ziv, Y. Shilina, E. Levi, S. Luski, D. Aurbach, Single-Wall Carbon Nanotube Doping in Lead-Acid Batteries: A New Horizon, *Applied Materials & Interfaces* 9 (2017) 3634–3643. DOI: 10.1021/acsami.6b13377
- [25] J. Furukawa, K. Smith, L.T. Lam, D.A.J. Rand, Towards sustainable road transport with the UltraBattery™ in: J. Garche, E. Karden, P.T. Moseley, D.A.J. Rand (Eds.), *Lead-Acid Batteries for Future Automobiles*, Elsevier Inc., Amsterdam, 2017, 349–391, DOI:10.1016/B978-0-444-63700-0.00012-X
- [26] J. Büngelera, E. Cattaneo, B. Riegel, D. U. Sauer, Advantages in energy efficiency of flooded lead-acid batteries when using partial state of charge operation, *J. Power Sources* 375 (2018) 53–58. DOI:10.1016/j.jpowsour.2017.11.050
- [27] R. Yahmadi, K. Brik, F.B. Ammar, Analysis approach of the formation current profiles impact on the lead acid battery manufacturing, *Recent Advances in Electrical and Electronic Engineering* 9 (2016) 231–240. DOI:10.2174/2352096509666161110105048
- [28] D.A.J. Rand, P.T. Moseley, Lead-acid battery fundamentals in: J. Garche, E. Karden, P.T. Moseley, D.A.J. Rand (Eds.), *Lead-Acid Batteries for Future Automobiles*, Elsevier Inc., Amsterdam, 2017, pp. 97–132, DOI:10.1016/B978-0-444-63700-0.00003-9
- [29] J. Hu, Y. Guo, Effects of electrolyte stratification on performances of AGM valve-regulated lead-acid batteries, *Electrochim. Acta* 52 (2007) 6734–6740, DOI:10.1016/j.electacta.2007.04.089
- [30] E. Ebner, A. Börger, M. Gelbke, E. Zena, M. Wieger, Temperature-dependent formation of vertical concentration gradients in lead-acid batteries under PSoC operation – Part 1: Acid stratification, *Electrochim. Acta* 90 (2013) 219–225, DOI:10.1016/j.electacta.2012.12.013
- [31] R.D. Prengaman, Current-collectors for lead-acid batteries in: J. Garche, E. Karden, P.T. Moseley, D.A.J. Rand (Eds.), *Lead-Acid Batteries for Future Automobiles*, Elsevier Inc., Amsterdam, 2017, 269–299, DOI:10.1016/B978-0-444-63700-0.00009-X
- [32] B. Hariprakash, S.A. Gaffoor, A.K. Shukla, Lead-acid batteries for partial-state-of-charge applications, *J. Power Sources* 191 (2009) 149–153. DOI:10.1016/j.jpowsour.2008.12.081
- [33] R. Inguanta, G. Ferrara, S. Piazza, C. Sunseri, Nanostructures fabrication by template deposition into anodic alumina membranes, *Chemical Engineering Transactions*, 17 (2009) 957–962. <http://doi.org/10.303/CET0917160>
- [34] R. Inguanta, G. Ferrara, S. Piazza, C. Sunseri, A New Route to Grow Oxide Nanostructures Based on Metal Displacement Deposition: Lanthanides Oxy/Hydroxides Growth, *Electrochim. Acta* 76 (2012) 77–87. DOI:10.1016/j.electacta.2012.04.146
- [35] M. Battaglia, S. Piazza, C. Sunseri, R. Inguanta, Amorphous silicon nanotubes via galvanic displacement deposition, *Electrochem. Commun.* 34 (2013) 134–137. DOI:10.1016/j.elecom.2013.05.041
- [36] L. Silipigni, F. Barreca, E. Fazio, F. Neri, T. Spanò, S. Piazza, C. Sunseri, R. Inguanta, Template Electrochemical Growth and Properties of Mo Oxide Nanostructures, *J. Phys. Chem. C* 118 (2014) 22299–22308. DOI:10.1021/jp505819j
- [37] G. Ferrara, R. Inguanta, S. Piazza, C. Sunseri, Characterization of SnCo nanowires grown into alumina template, *Electrochem. Solid State Lett.* 12 (2009) K17–K20, DOI:10.1149/1.3059545.
- [38] L. Genovese, C. Cocchiara, S. Piazza, C. Sunseri, R. Inguanta, Electrochemical deposition of Ag<sub>2</sub>Se nanostructures, *Mater. Res. Bull.* 86 (2017) 10–18. DOI:10.1016/j.materresbull.2016.09.033
- [39] A. Moncada, R. Inguanta, S. Piazza, C. Sunseri, Nano-structured PbO<sub>2</sub> electrode for lead-acid battery, pp. 161–164 *Proceedings of 9th International Conference on Lead-Acid Batteries LABAT'2014 Albena, Bulgaria June 10–13, 2014*

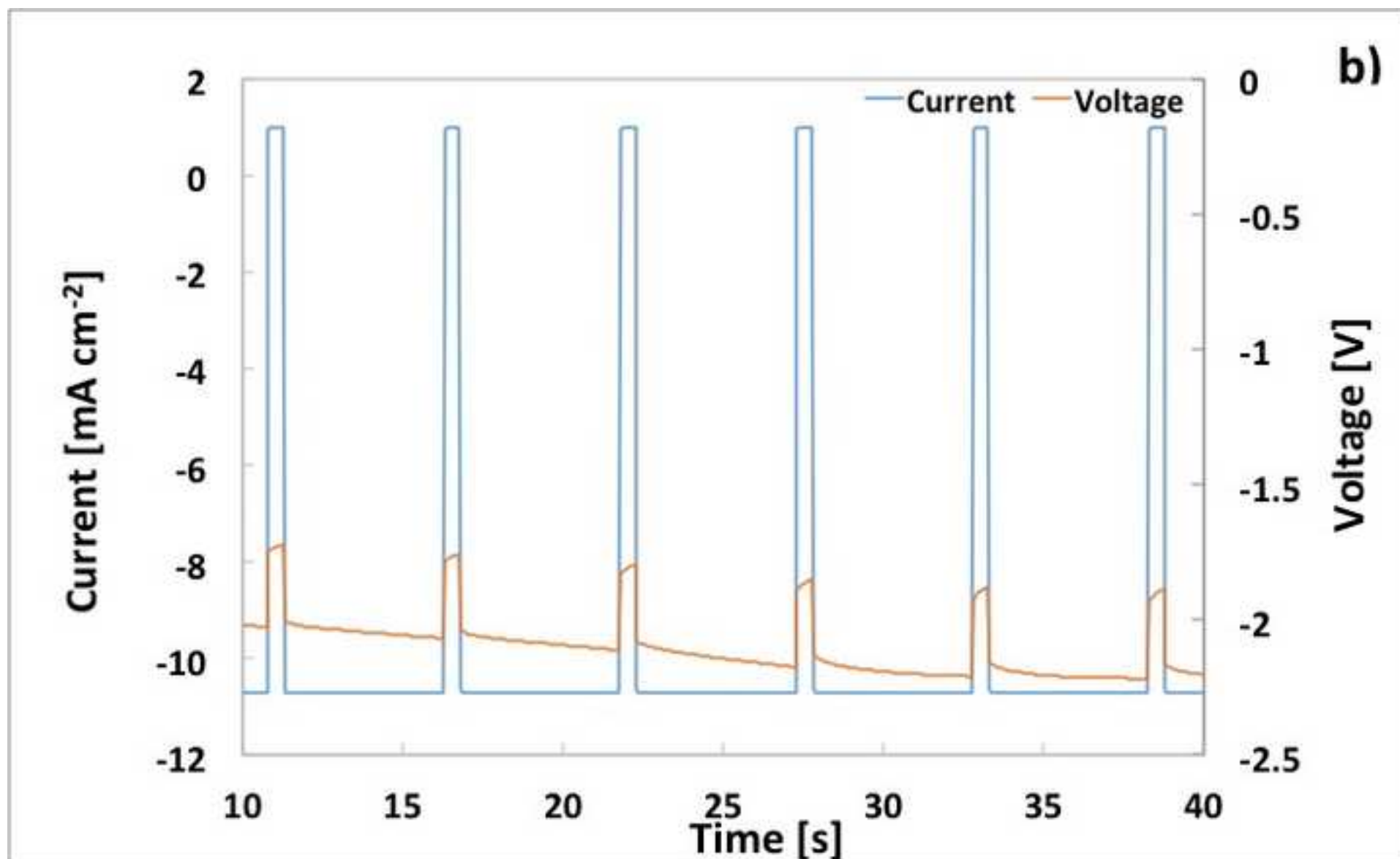


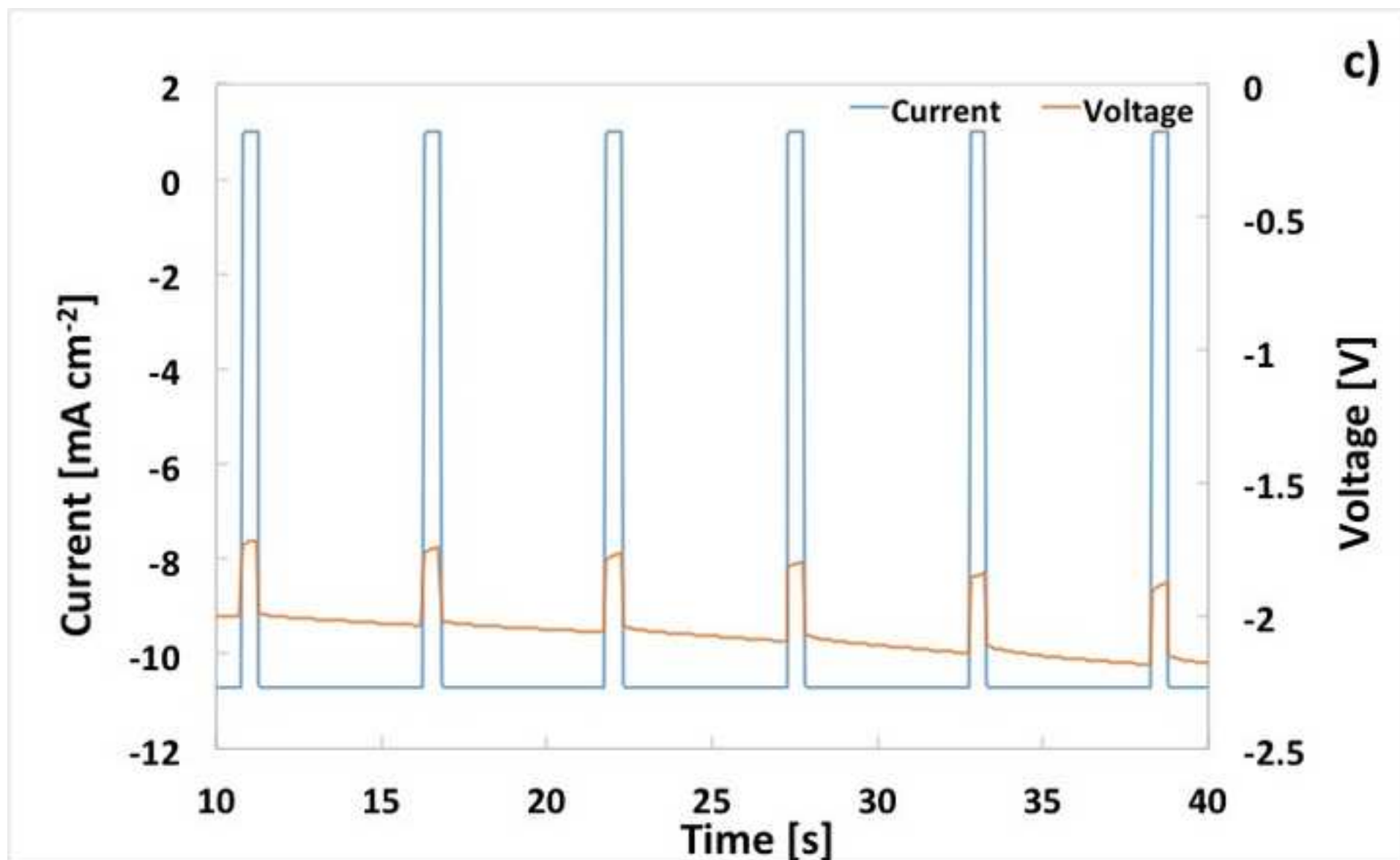
- [40] A. Moncada, M.C. Mistretta, S. Randazzo, S. Piazza, C. Sunseri, R. Inguanta, High-performance of PbO<sub>2</sub> nanowire electrodes for lead-acid battery, *J. Power Sources* 256 (2014) 72-79. DOI:10.1016/j.jpowsour.2014.01.050
- [41] A. Moncada, R. Inguanta, S. Piazza, C. Sunseri, Performance of Nanostructured Electrode in Lead Acid Battery, *Chemical Engineering Transactions* 43 (2015) 751-756. <http://doi.org/10.3303/CET1543126>
- [42] A. Moncada, S. Piazza, C. Sunseri, R. Inguanta, Recent improvements in PbO<sub>2</sub> nanowire electrodes for lead-acid battery, *J. Power Sources* 275 (2015) 181-188. DOI:10.1016/j.jpowsour.2014.10.189
- [43] R. Inguanta, S. Randazzo, A. Moncada, M.C. Mistretta, S. Piazza, C. Sunseri, Growth and Electrochemical Performance of Lead and Lead Oxide Nanowire Arrays as Electrodes for Lead-Acid Batteries, *Chemical Engineering Transactions* 32 (2013) 2227-2232. DOI:10.3303/CET1332372
- [44] M.G. Insinga, A. Moncada, R.L. Oliveri, F. Ganci, S. Piazza, C. Sunseri, R. Inguanta, Nanostructured Pb Electrode for Innovative Lead-acid Battery, *Chemical Engineering Transactions* 60 (2017) 49-54. DOI: 10.3303/CET1760009
- [45] R. Inguanta, E. Rinaldo, S. Piazza, C. Sunseri, Lead Nanowires for Microaccumulators Obtained Through Indirect Electrochemical Template Deposition, *Electrochem. and Solid-State Lett.* 13(1) (2009) K1-K4. <http://doi.org/10.1149/1.3246944>
- [46] R. Inguanta, S. Piazza, C. Sunseri, Growth and Characterization of Ordered PbO<sub>2</sub> Nanowire Arrays, *J. Electrochem. Soc.* 155 (2008) K205-K210. DOI:10.1149/1.2988728
- [47] M. Jordan, Electrodeposition of Lead and Lead Alloys, in: M. Schlesinger, M. Paunovic (Eds.), *Modern Electroplating*, John Wiley & Sons, Inc., Hoboken, New Jersey, 2010, pp. 249-263.
- [48] M. Saravan, M. Ganesan, S. Ambalavanan, An in situ generated carbon as integrated conductive additive for hierarchical negative plate of lead-acid battery, *J. Power Sources* 251 (2014) 20-29, DOI:10.1016/j.jpowsour.2013.10.143
- [49] N. Sugumaran, P. Everill, S.W. Swogger, D.P. Dubey, Lead acid battery performance and cycle life increased through addition of discrete carbon nanotubes to both electrodes, *J. Power Sources* 279 (2015) 281-293, DOI:10.1016/j.jpowsour.2014.12.117
- [50] D. Pavlov, T. Rogachev, P. Nikolov, G. Petkova, Mechanism of action of electrochemically active carbons on the processes that take place at the negative plates of lead-acid batteries, *J. Power Sources* 191 (2009) 58-75. DOI:10.1016/j.jpowsour.2008.11.056
- [51] D.G. Enosa, S.R. Ferreira, H.M. Barkholtz, W. Baca, S. Fenstermacher, Understanding Function and Performance of Carbon Additives in Lead-Acid Batteries, *J. Electrochem. Soc.* 164(13) (2017) A3276-A3284. DOI: 10.1149/2.1031713jes
- [52] J. Setteleina, H. Lormann, G. Sextl, Evaluating the lead affinity of graphite additives in lead-acid batteries by electrochemical deposition, *Electrochim. Acta* 233 (2017) 173-180. DOI:10.1016/j.electacta.2017.03.034
- [53] X. Lang, Y. Zhao, K. Cai, L. Lic, Q. Zhanga, H. Wu, Preparation of four basic lead sulfate nano-rods additives and effect on the electrochemical performance of lead-acid battery, *J. Energy Storage* 13 (2017) 137-142. DOI:10.1016/j.est.2017.07.009
- [54] D. Pavlov, P. Nikolov, T. Rogachev, Influence of carbons on the structure of the negative active material of lead-acid batteries and on battery performance, *J. Power Sources* 196 (2011) 5155-5167, DOI:10.1016/j.jpowsour.2011.02.014
- [55] X. Lang, Y. Xiao, K. Cai, L. Li, Q. Zhang, R. Yang, High-performance porous lead/graphite composite electrode for bipolar lead-acid batteries, *International Journal of Energy Research* 41 (2017) 1504-1509, DOI:10.1002/er.3729

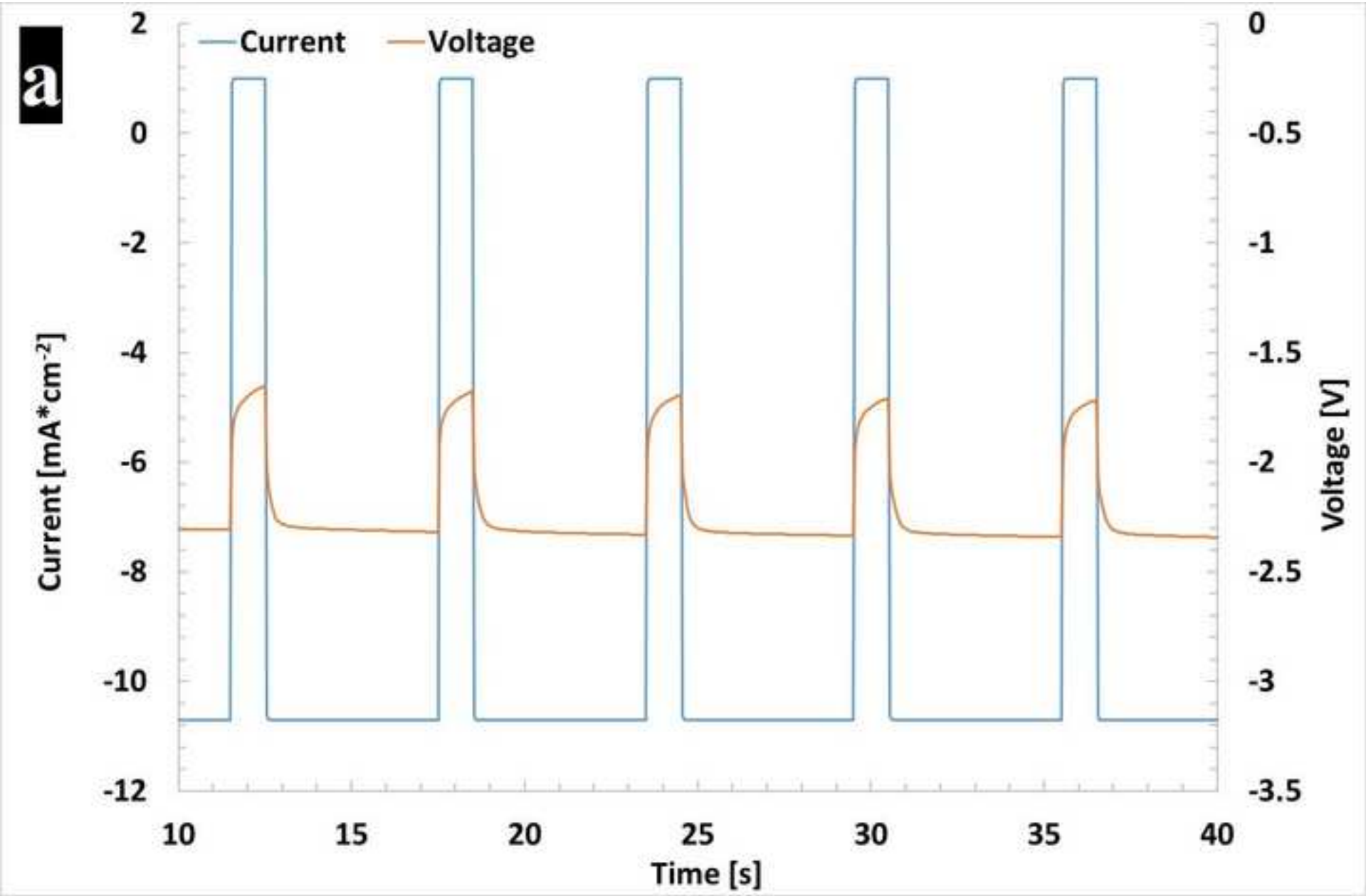
- [56] Y. Chen, B. Chen, L. Ma, Y. Yuan, Effect of carbon foams as negative current collectors on partial-state-of-charge performance of lead acid batteries, *Electrochem. Comm.* 10 (2008) 1064-1066, DOI: 10.1016/j.elecom.2008.05.009
- [57] E. Gyenge J. Jung, B. Mahato, Electroplated reticulated vitreous carbon current collectors for lead–acid batteries: opportunities and challenges, *J. Power Sources* 113 (2003) 388–395. DOI: 10.1016/S0378-7753(02)00553-0
- [58] K.-T. Hao, X.-J. Lü, M. Jia, B. Hong, L.-X. Jiang, J. Fang, Y.-Q. Lai, J. Li, Y.-X. Liu, Preparation and performance of Al/Pb composite material for lead-acid battery negative grid, *Zhongguo Youse Jinshu Xuebao/Chinese Journal of Nonferrous Metals* 23 (2013) 1591-1597
- [59] S. Zhang, H. Zhang, J. Cheng, W. Zhang, G. Cao, H. Zhao, Y. Yang, Novel polymer-graphite composite grid as a negative current collector for lead-acid batteries, *J. Power Sources* 334 (2016) 31-38. DOI:10.1016/j.jpowsour.2016.09.097
- [60] J.A. Von Fraunhofer, Electrodeposition of Lead, in: A.T. Kuhn (ed.), *The Electrochemistry of Lead*, Academic Press, London, 1979, pp.135-158.
- [61] R. Inguanta, G. Ferrara, S. Piazza, C. Sunseri, Fabrication and characterization of metal and metal oxide nanostructures grown by metal displacement deposition into anodic alumina membranes, *Chemical Engineering Transactions*, 24 (2011) 199-204 DOI:10.3303/CET/11241034
- [62] J. O. Bockris, A.K. N. Reddy, M. Gamboa-Aldeco, *Modern Electrochemistry 2A*, Kluwer Academic/Plenum Publishers, New York, 1998, pp.1338-1339
- [63] D. Pavlov, *Lead-acid batteries: Science and technology a handbook of lead-acid battery technology and its influence on the product*, Elsevier, Amsterdam, 2017.
- [64] X. Chen, J. Chen, X. Ouyang, Y. Song, R. Xu, P. Jiang, Water Droplet Spreading and Wicking on Nanostructured Surfaces, *Langmuir* 33(27) (2017) 6701-6707, DOI:10.1021/acs.langmuir.7b01223
- [65] C.K. Wemp, V.P. Carey, Water Wicking and Droplet Spreading on Randomly Structured Thin Nanoporous Layers, *Langmuir* 33(50) (2017) 14513-14525 DOI:10.1021/acs.langmuir.7b03687
- [66] T.N. Das, Saturation Concentration of Dissolved O<sub>2</sub> in Highly Acidic Aqueous Solutions of H<sub>2</sub>SO<sub>4</sub>, *Ind. Eng. Chem. Res.* 44 (2005) 1660-1664.
- [67] A.N. Fleming, J.A. Harrison, The Aqueous System Pb<sup>2+</sup>/Pb, in: A.T. Kuhn (ed.), *The Electrochemistry of Lead*, Academic Press, London, 1979, pp.1-28.
- [68] M. Hayes, A.T. Kuhn, Hydrogen Evolution and Oxygen Reduction on Lead, in: A.T. Kuhn (ed.), *The Electrochemistry of Lead*, Academic Press, London, 1979, pp.199-213.
- [69] A. J. Salkind, A. G. Cannone, F. A. Trumbure in *Handbook of Batteries* D. Linden, T. B. Reddy editors, McGraw-Hill, New York, 2002.
- [70] Y. Chen, H. Huang, H. Ma, D. Kong, *Electrochim. Acta* 88 (2013) 79-85
- [71] E. Budevski, G. Staikov, W.J. Lorenz, Electrocrystallization Nucleation and growth phenomena. *Electrochimica Acta* 45 (2000) 2559–2574. DOI:10.1016/S0013-4686(00)00353-4
- [72] L. Rodriguez-Sanchez, M.C. Blanco, M.A. Lopez-Quintela, Electrochemical Synthesis of Silver Nanoparticles, *Journal Physical Chemistry B*, 104 (2000) 9683-9688, Table 3. DOI:10.1021/jp001761r



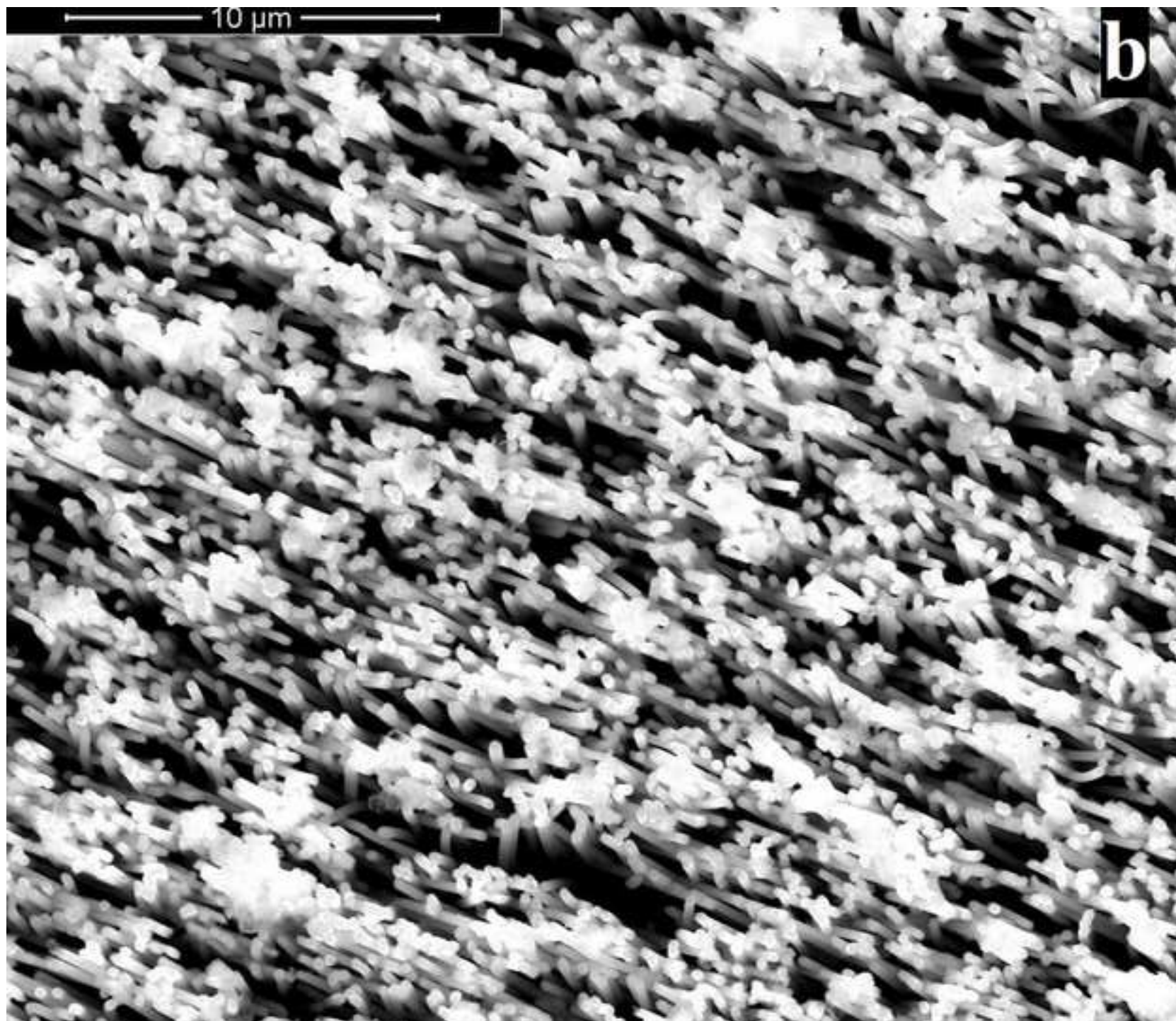




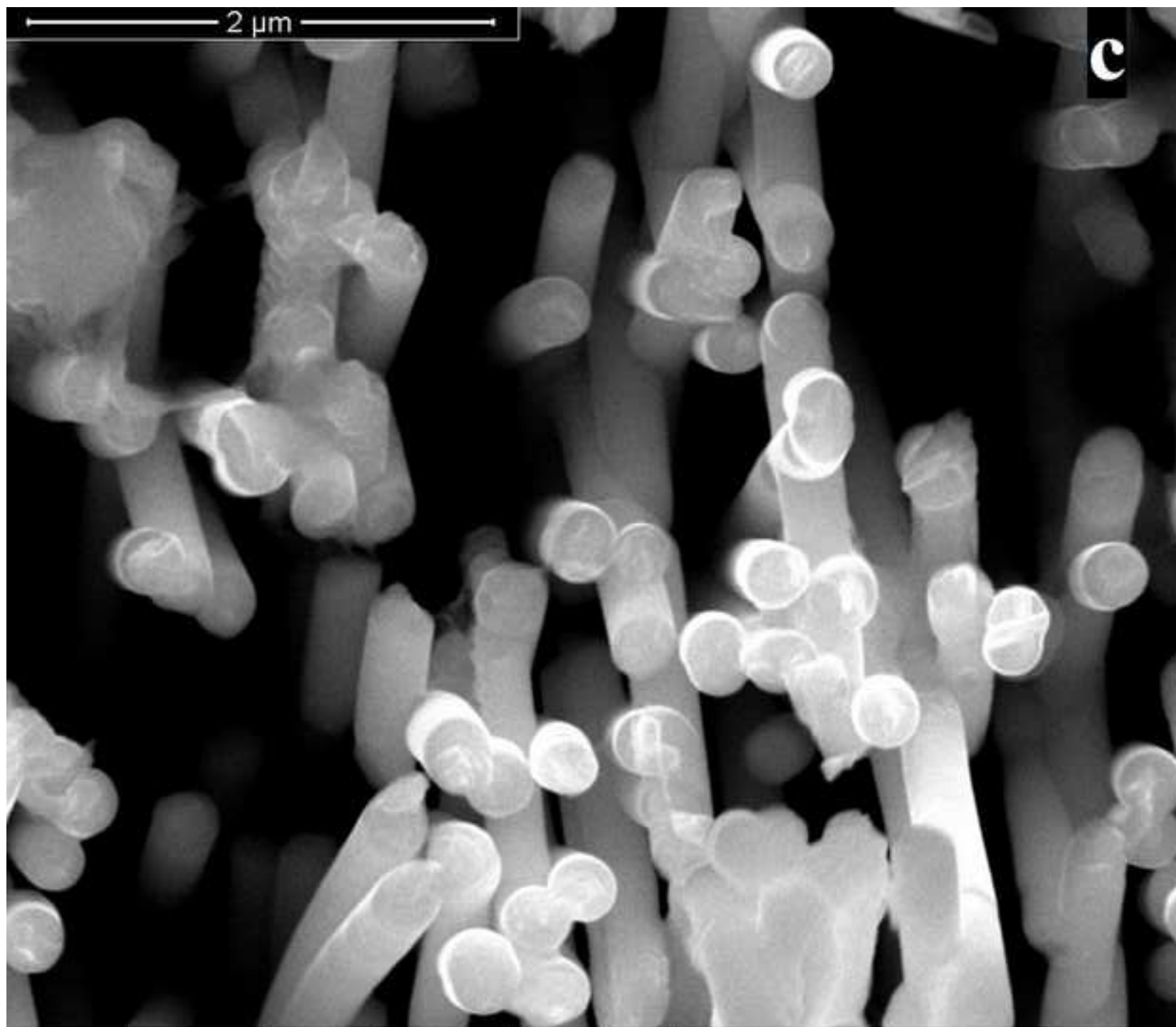




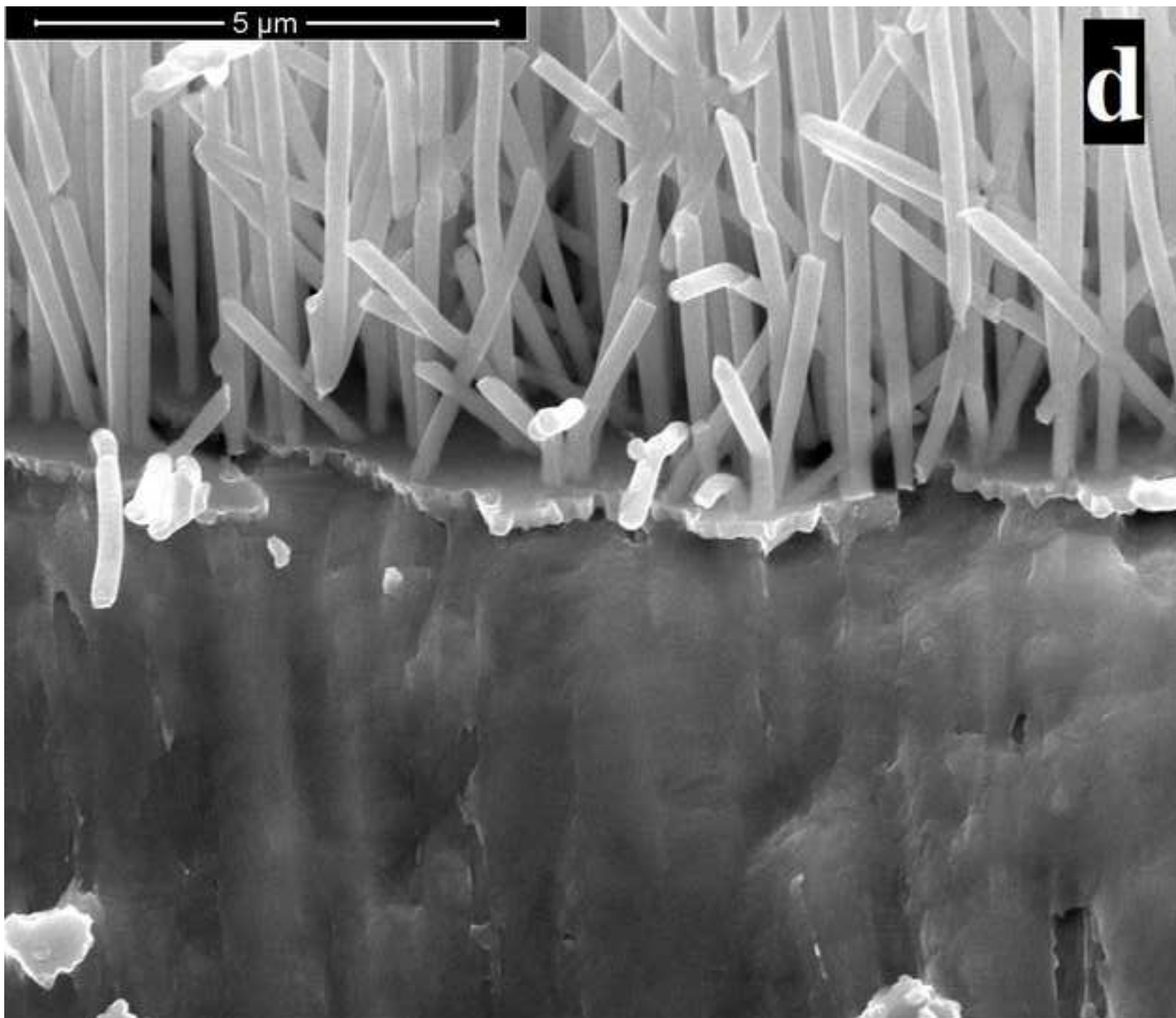
Figure(s) - provided separately  
[Click here to download high resolution image](#)

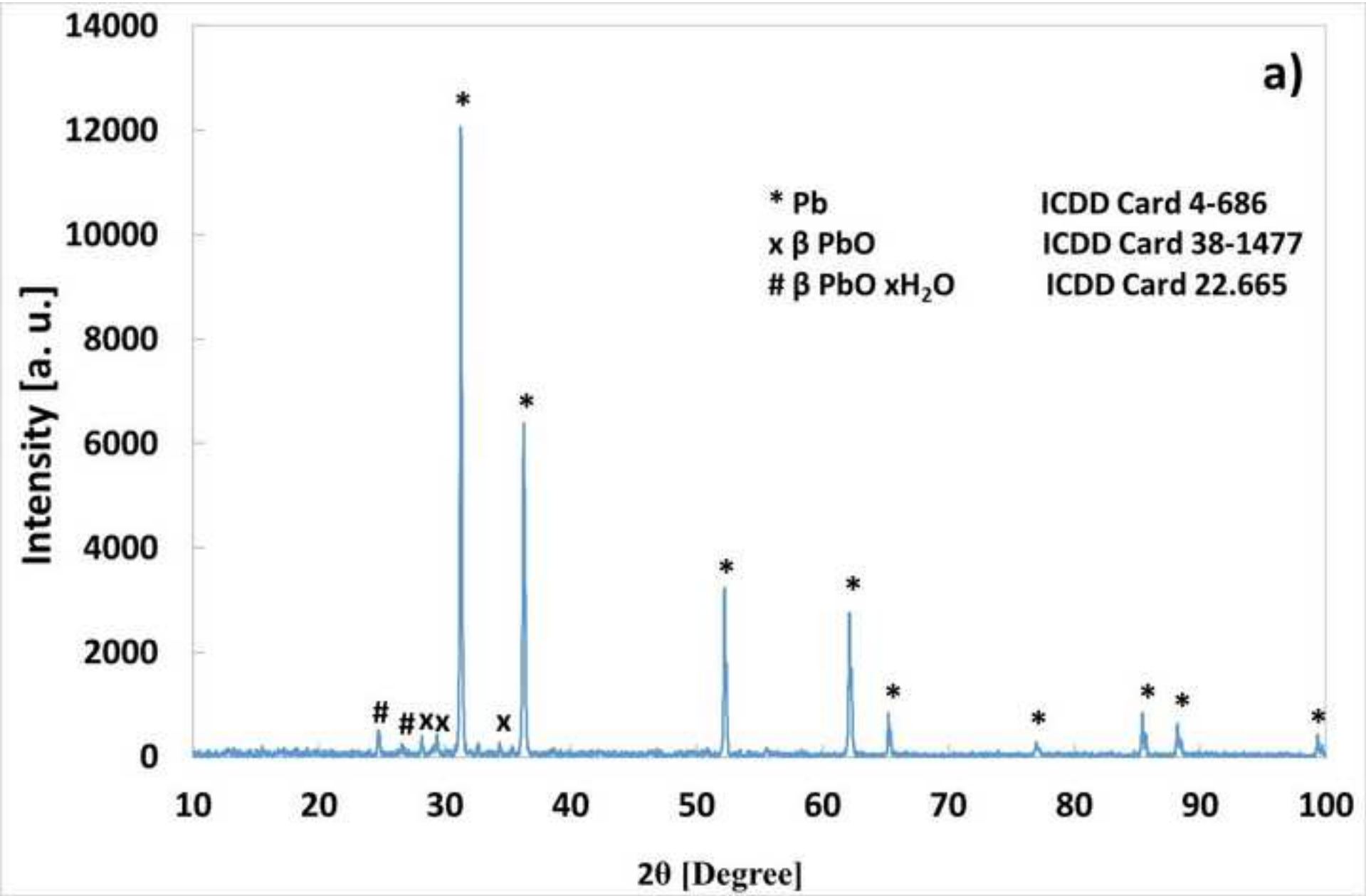




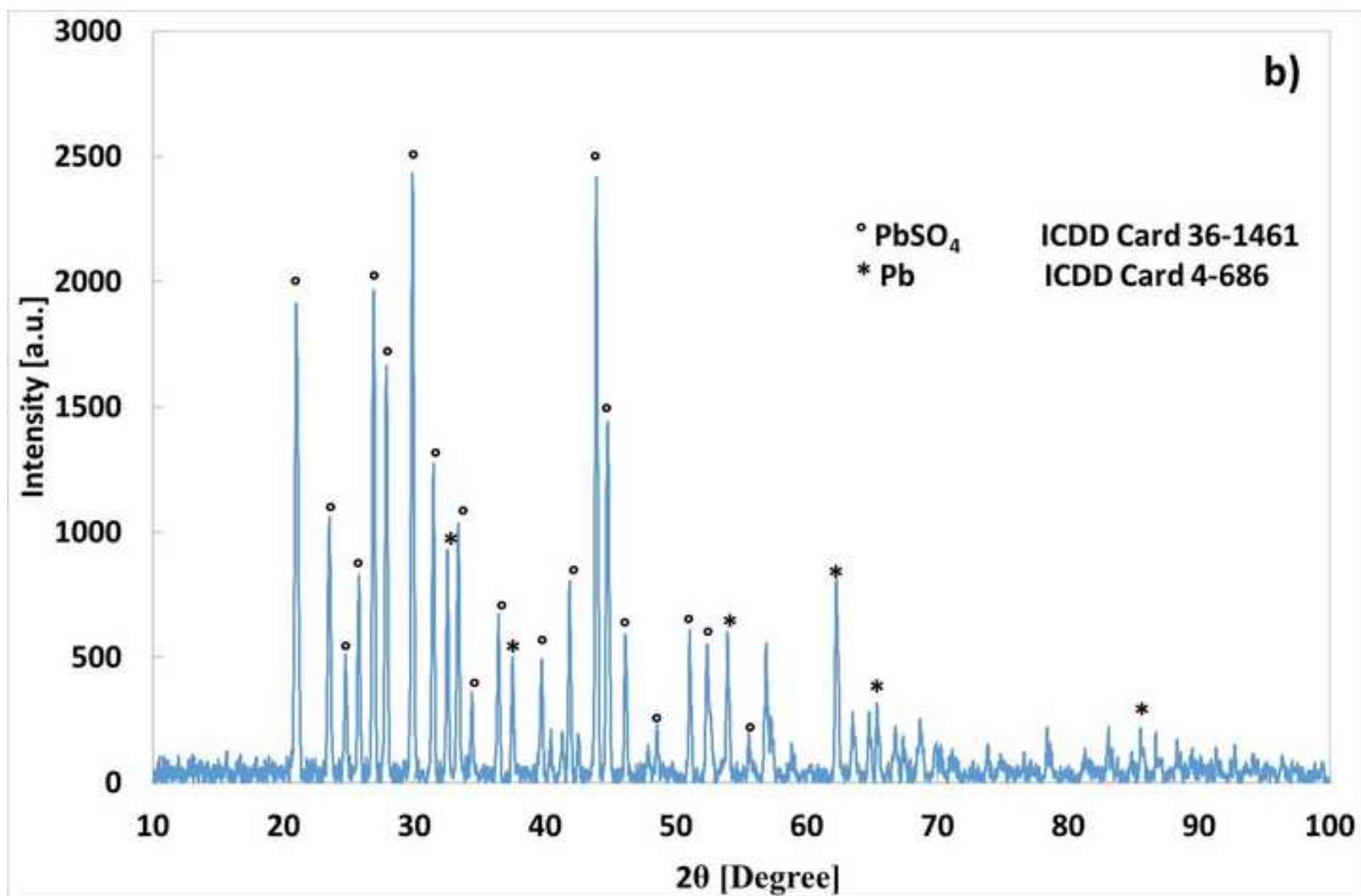


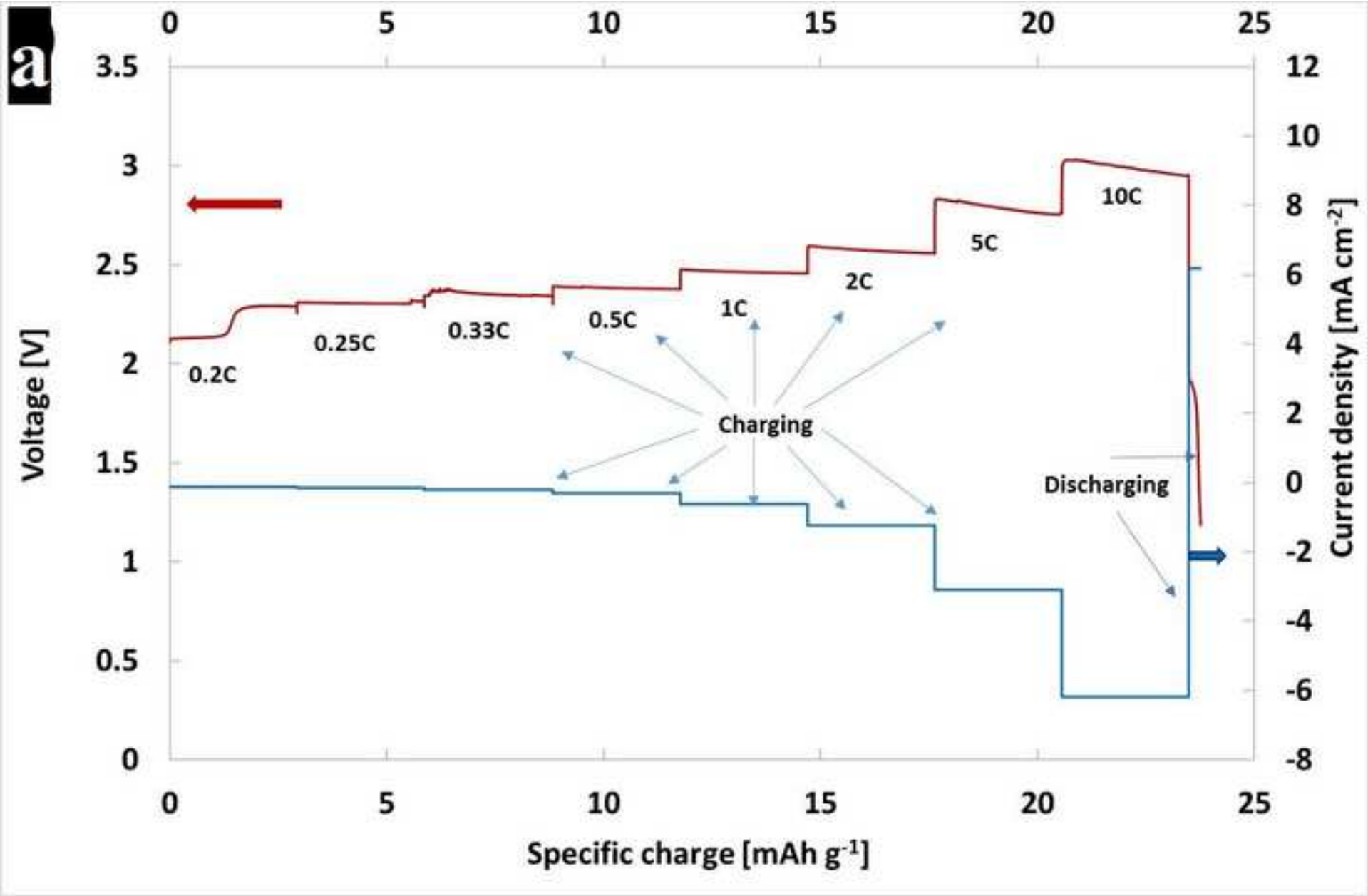
Figure(s) - provided separately  
[Click here to download high resolution image](#)

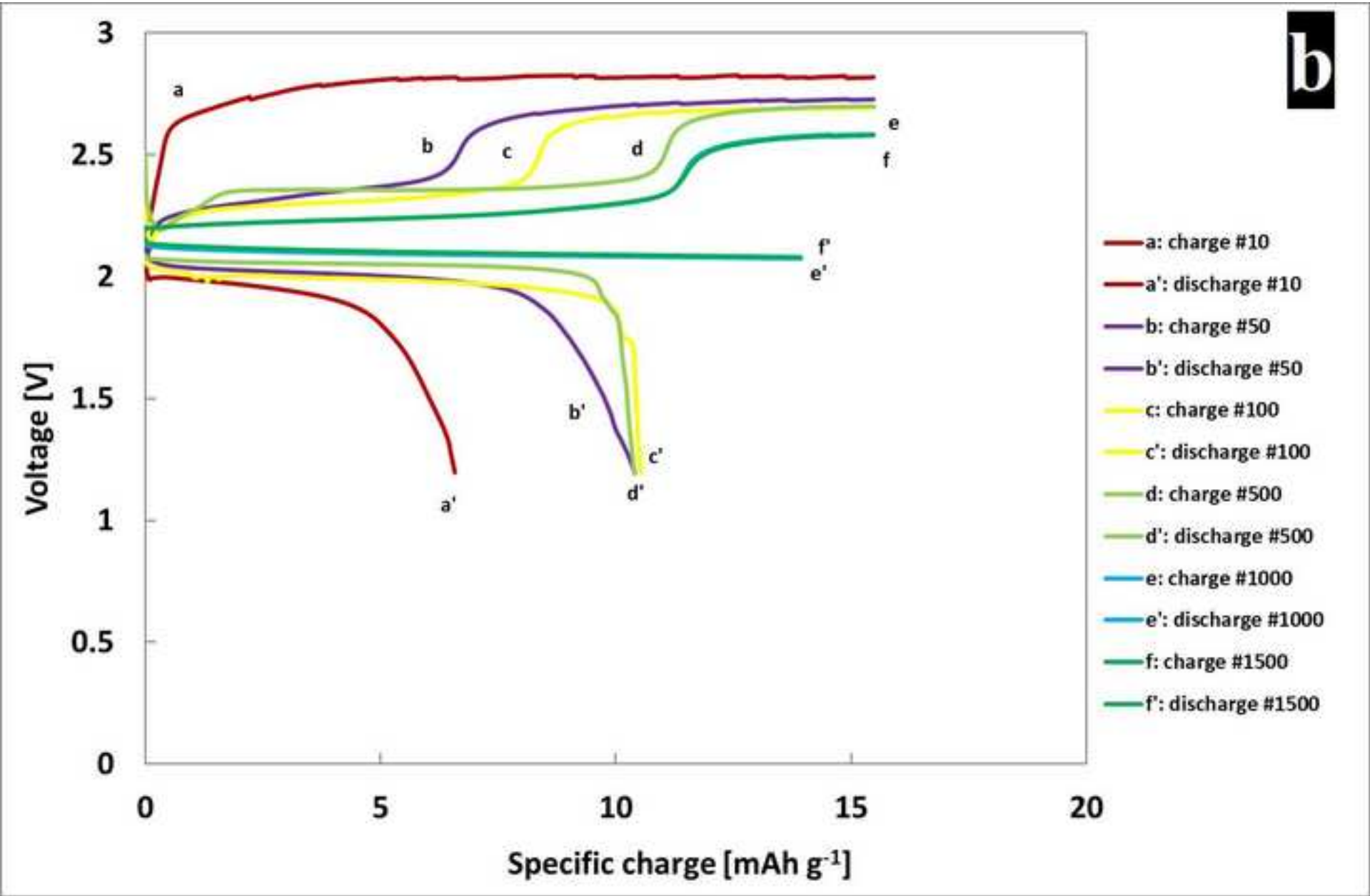


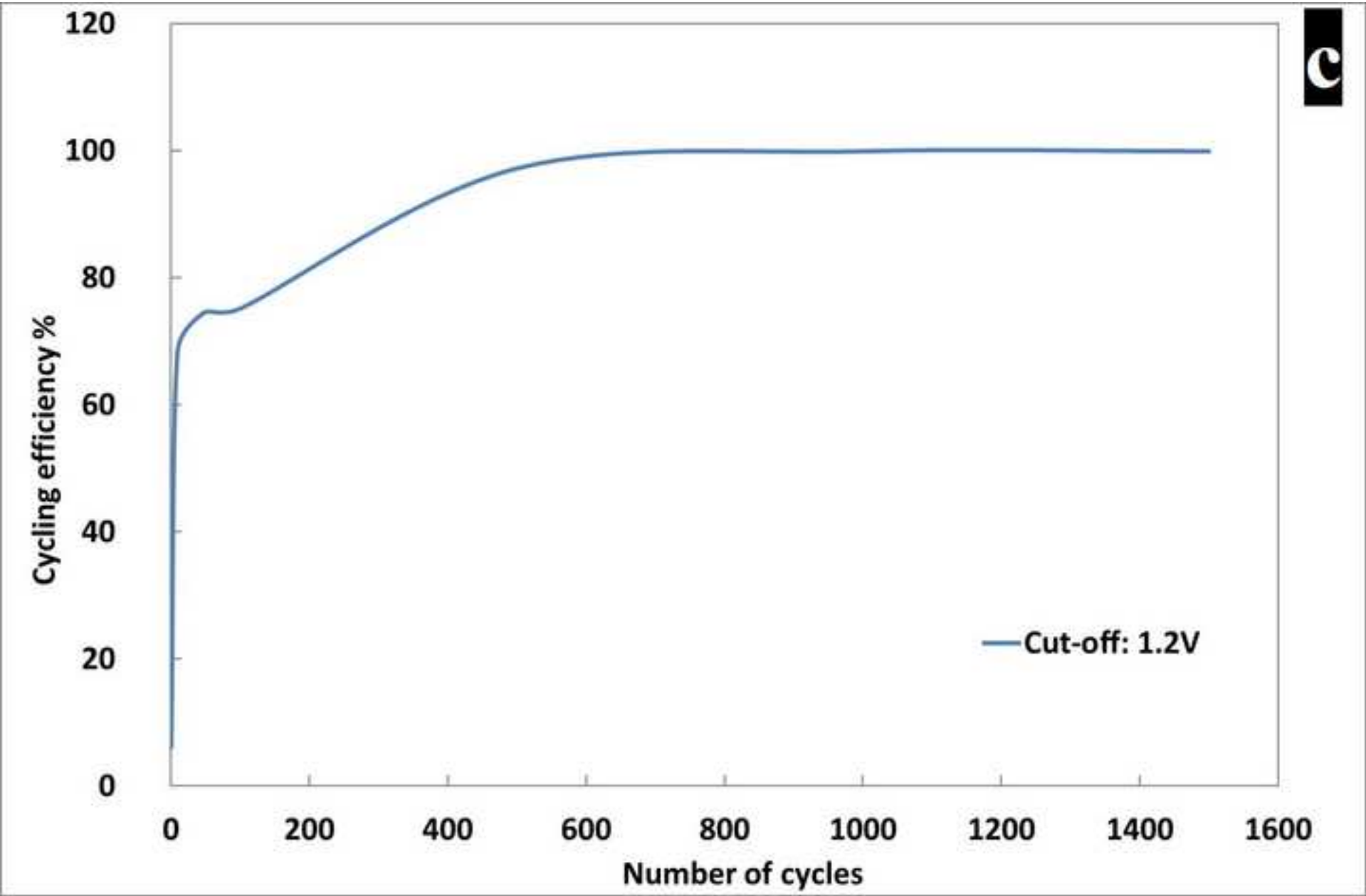


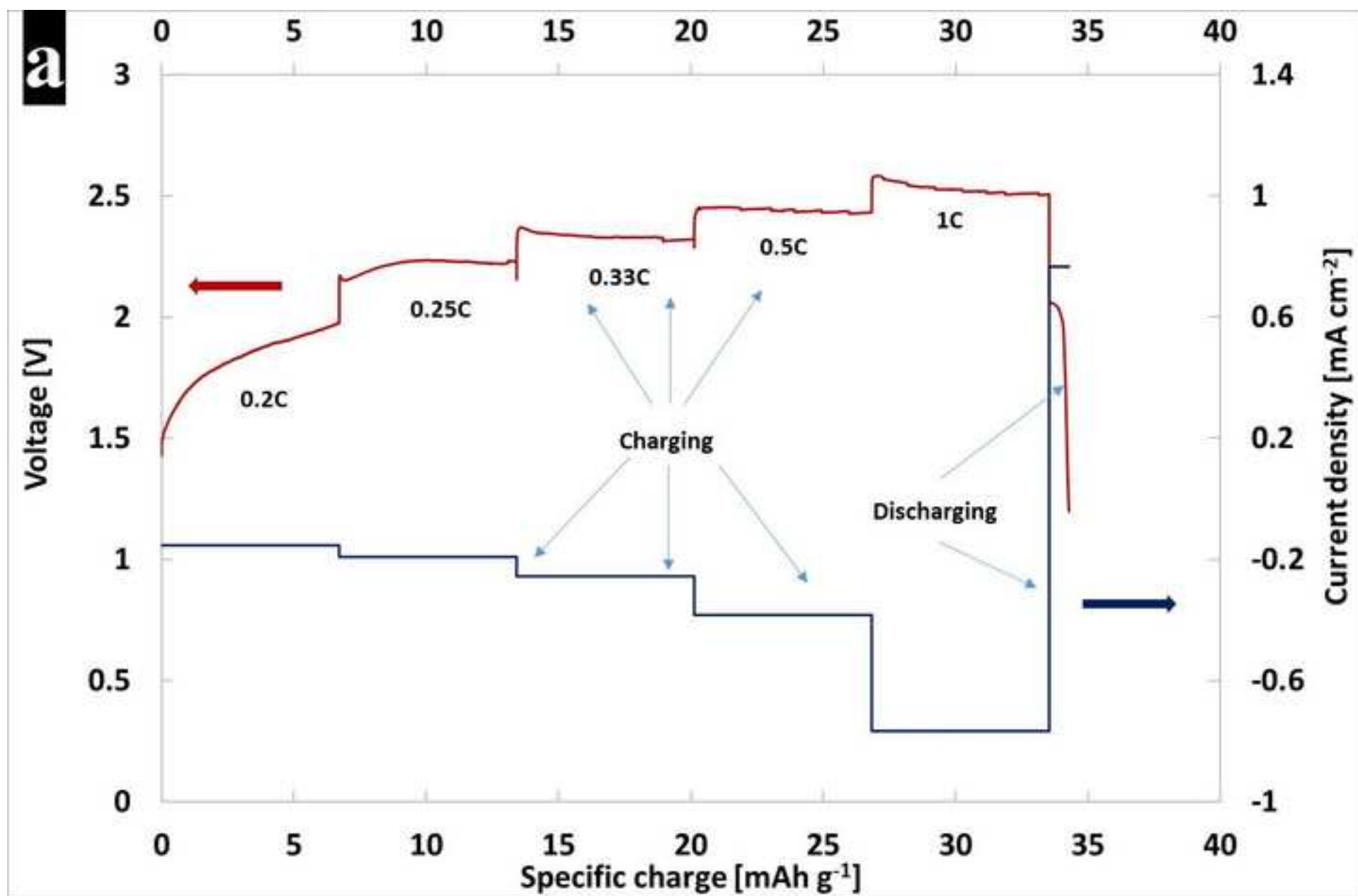


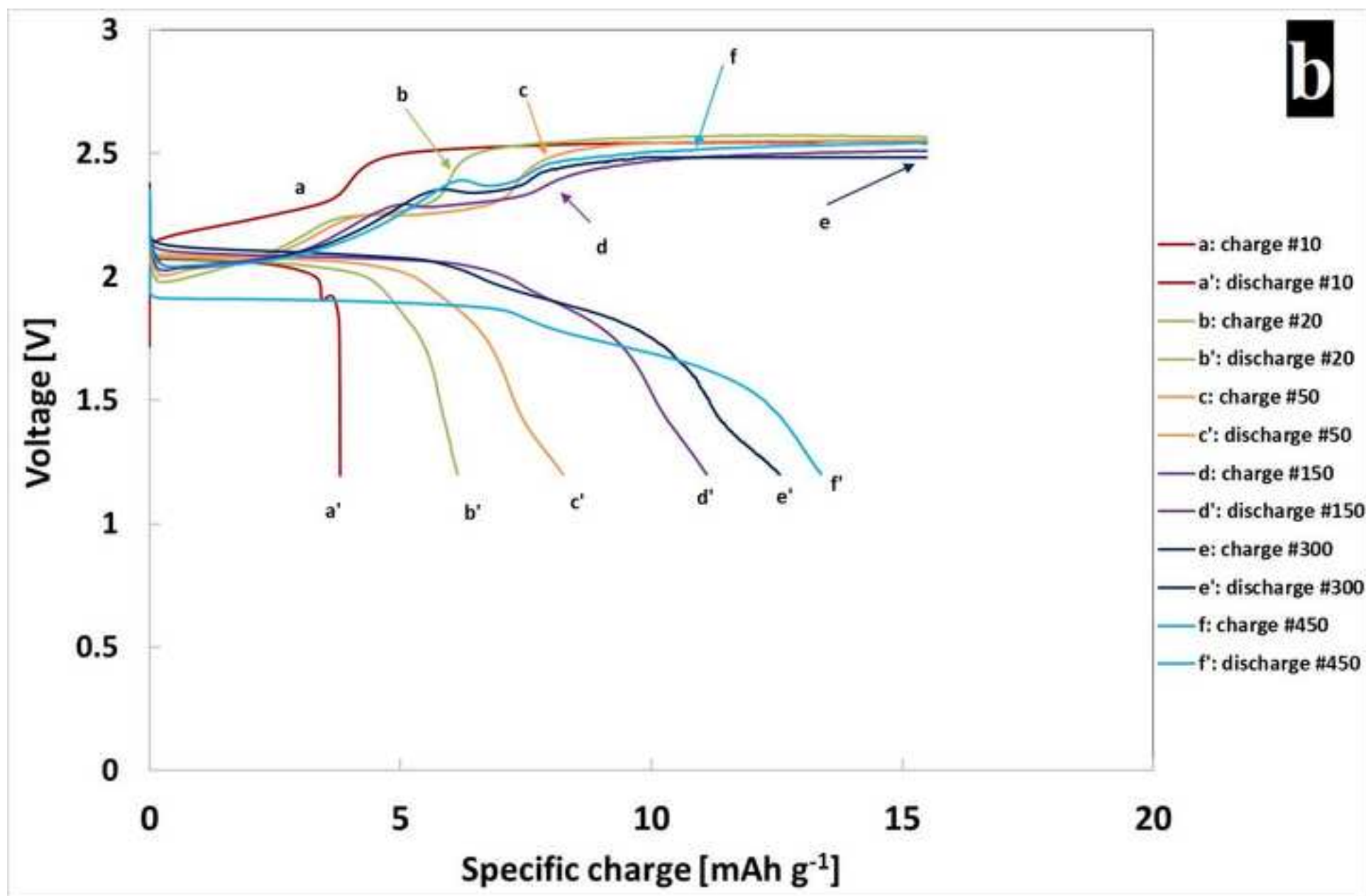


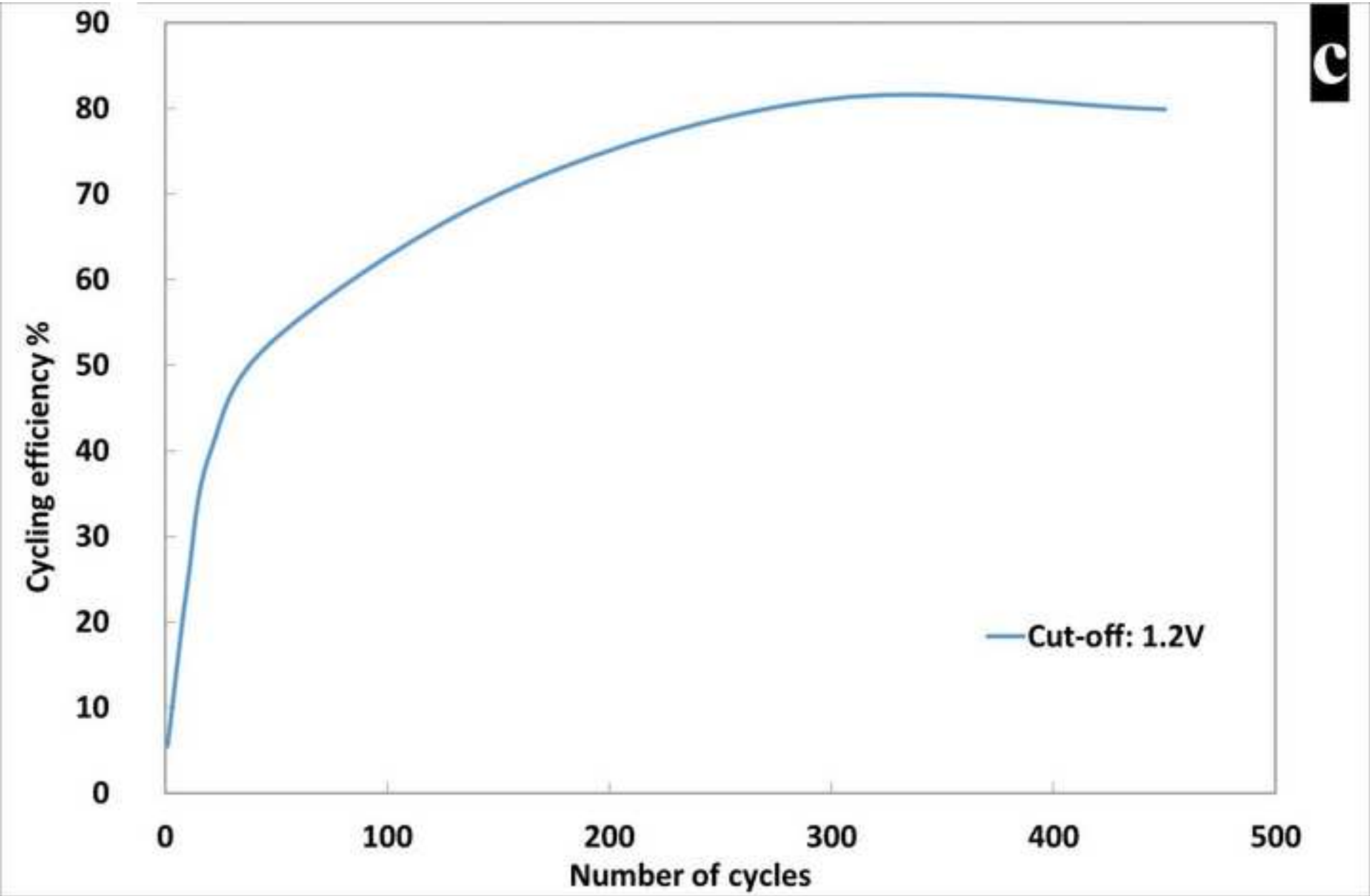








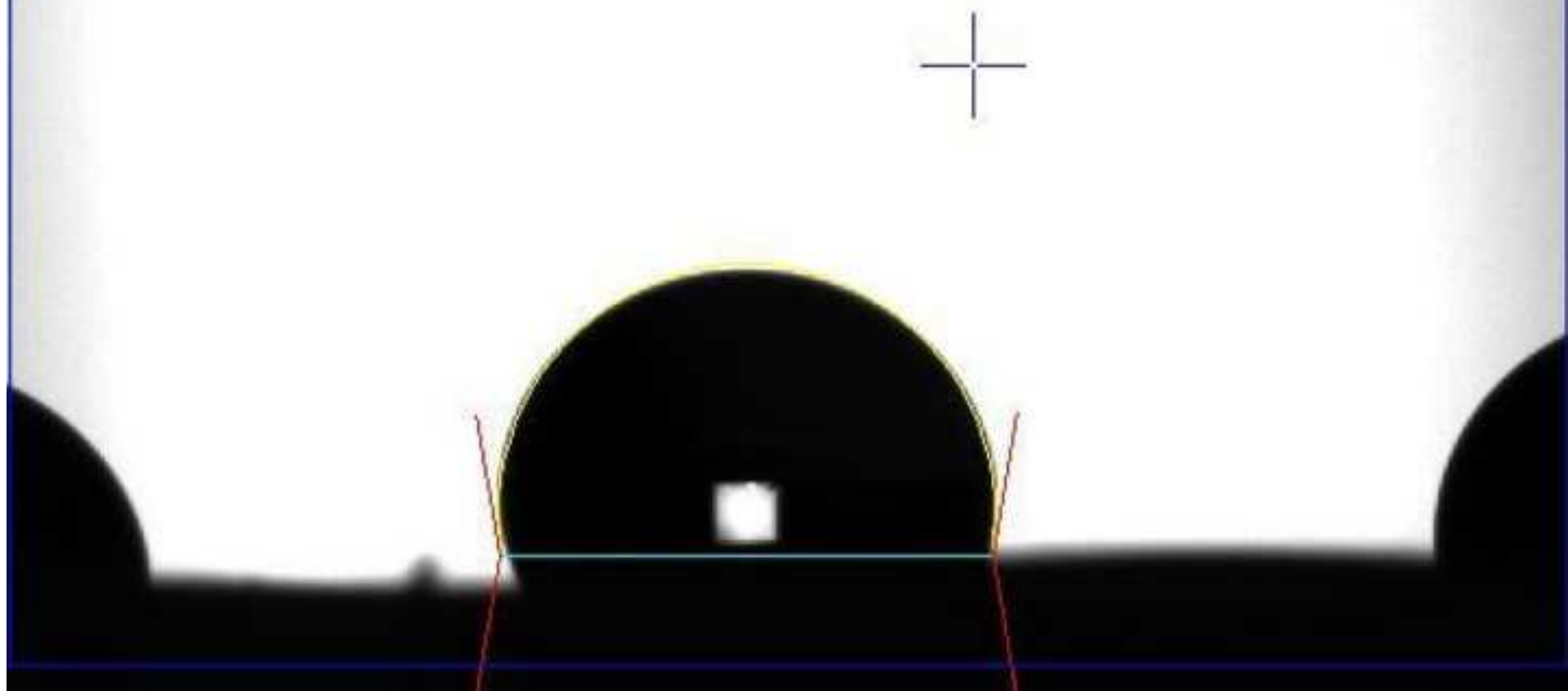




Angle = 99.63 degrees  
Base Width = 2.9632mm

a

as prepared





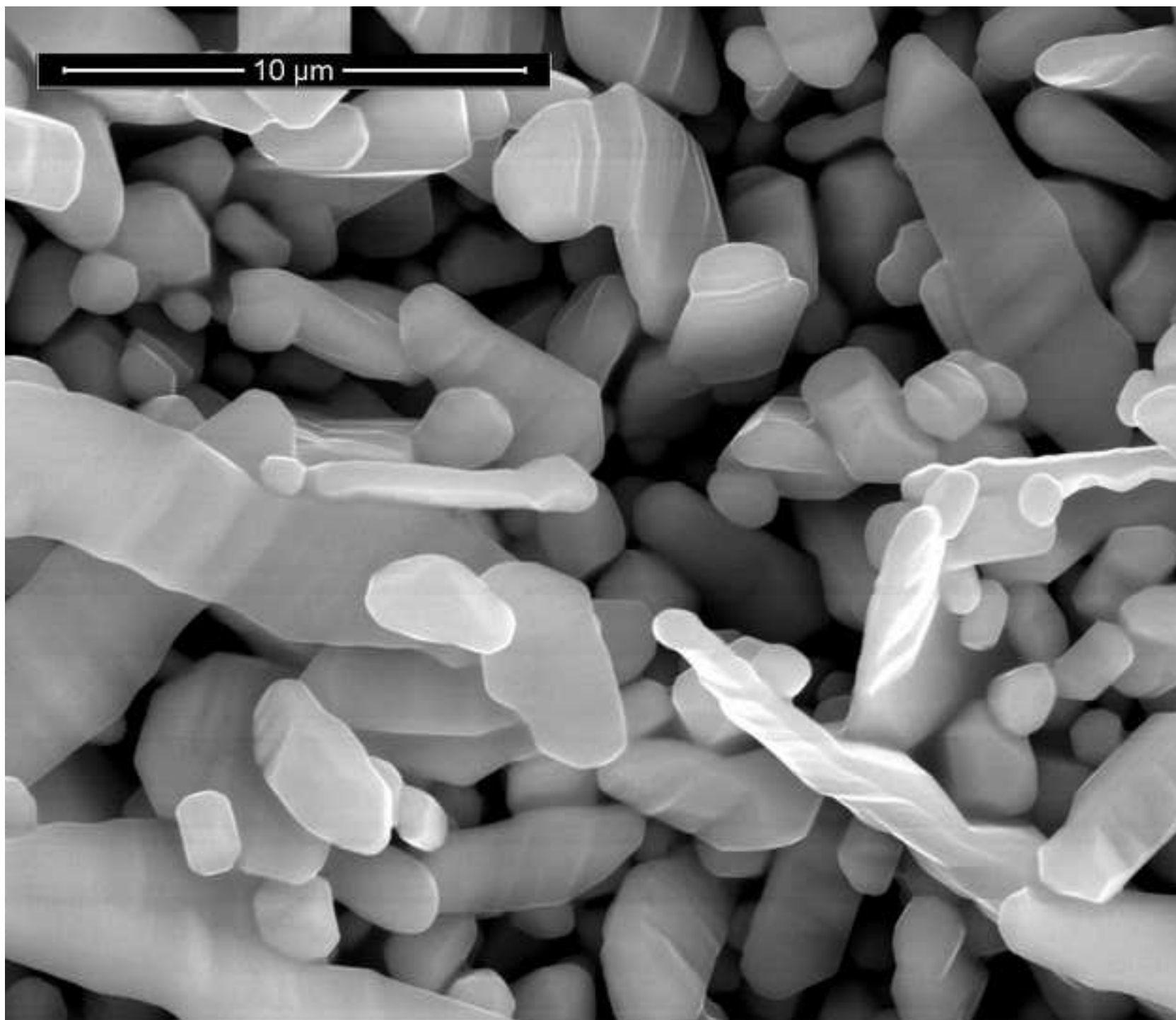
Angle = 86.75 degrees  
Base Width = 3.0955mm

**b**

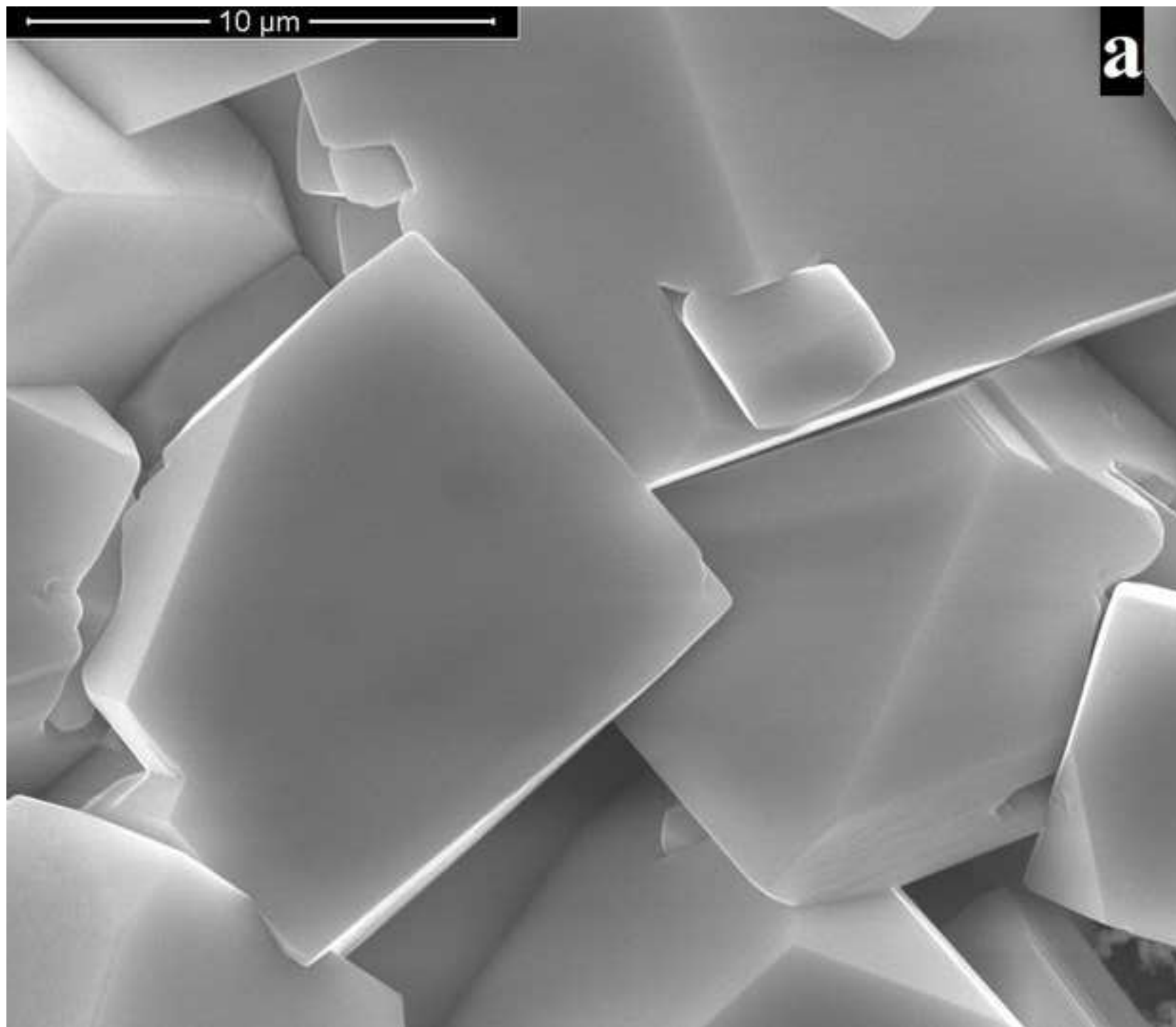
**after 50 cycles**

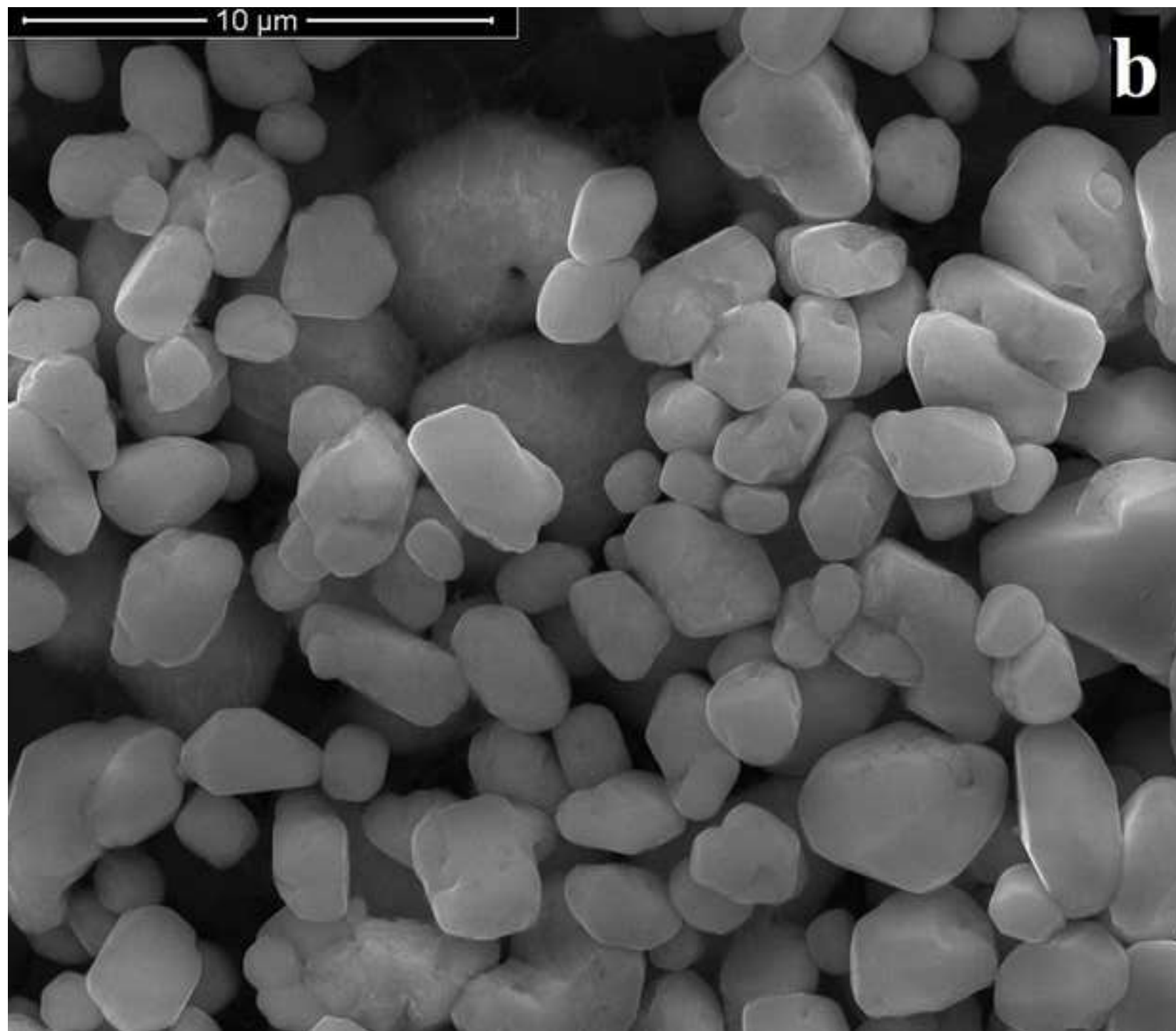


Figure(s) - provided separately  
[Click here to download high resolution image](#)

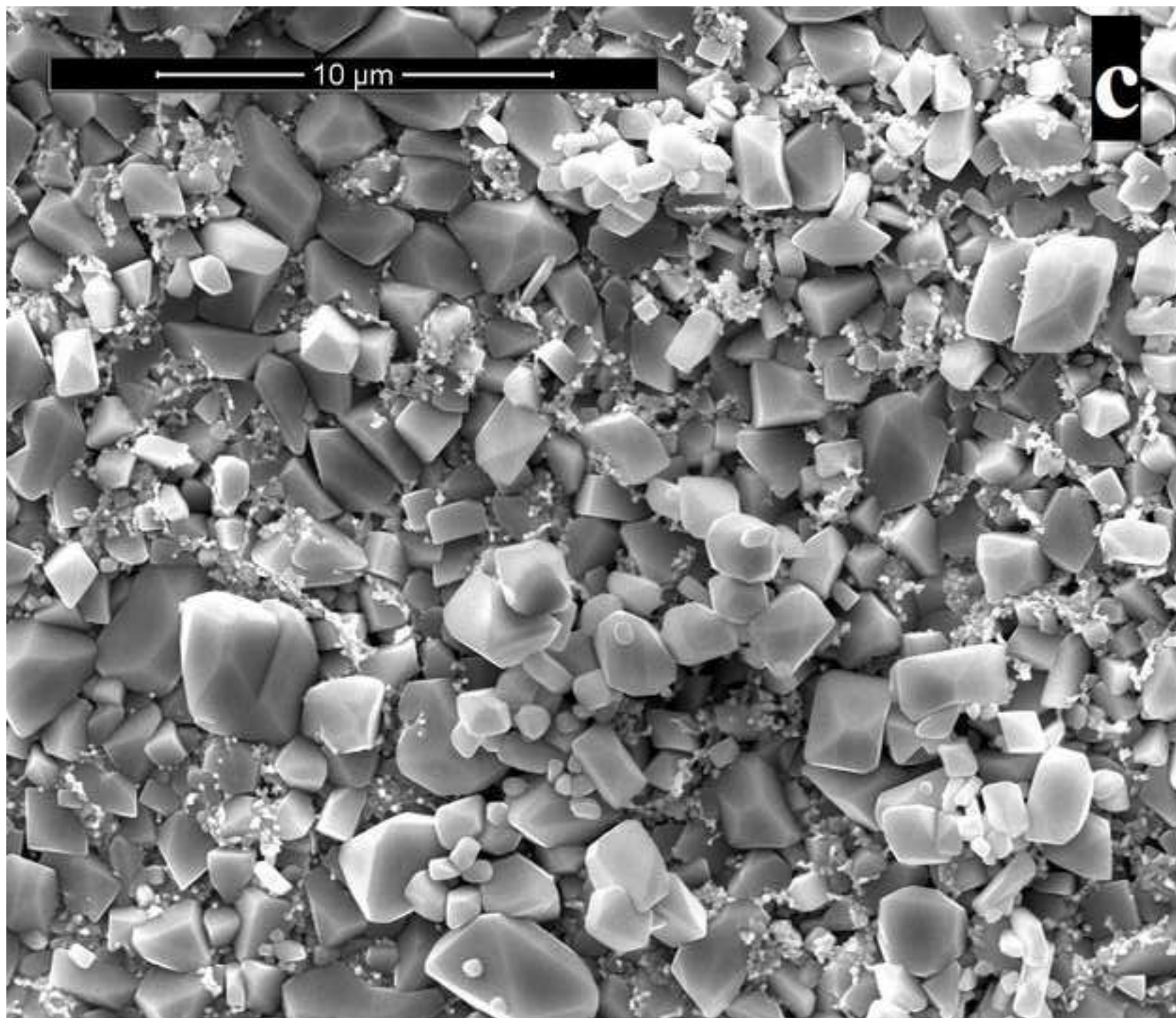


Figure(s) - provided separately  
[Click here to download high resolution image](#)









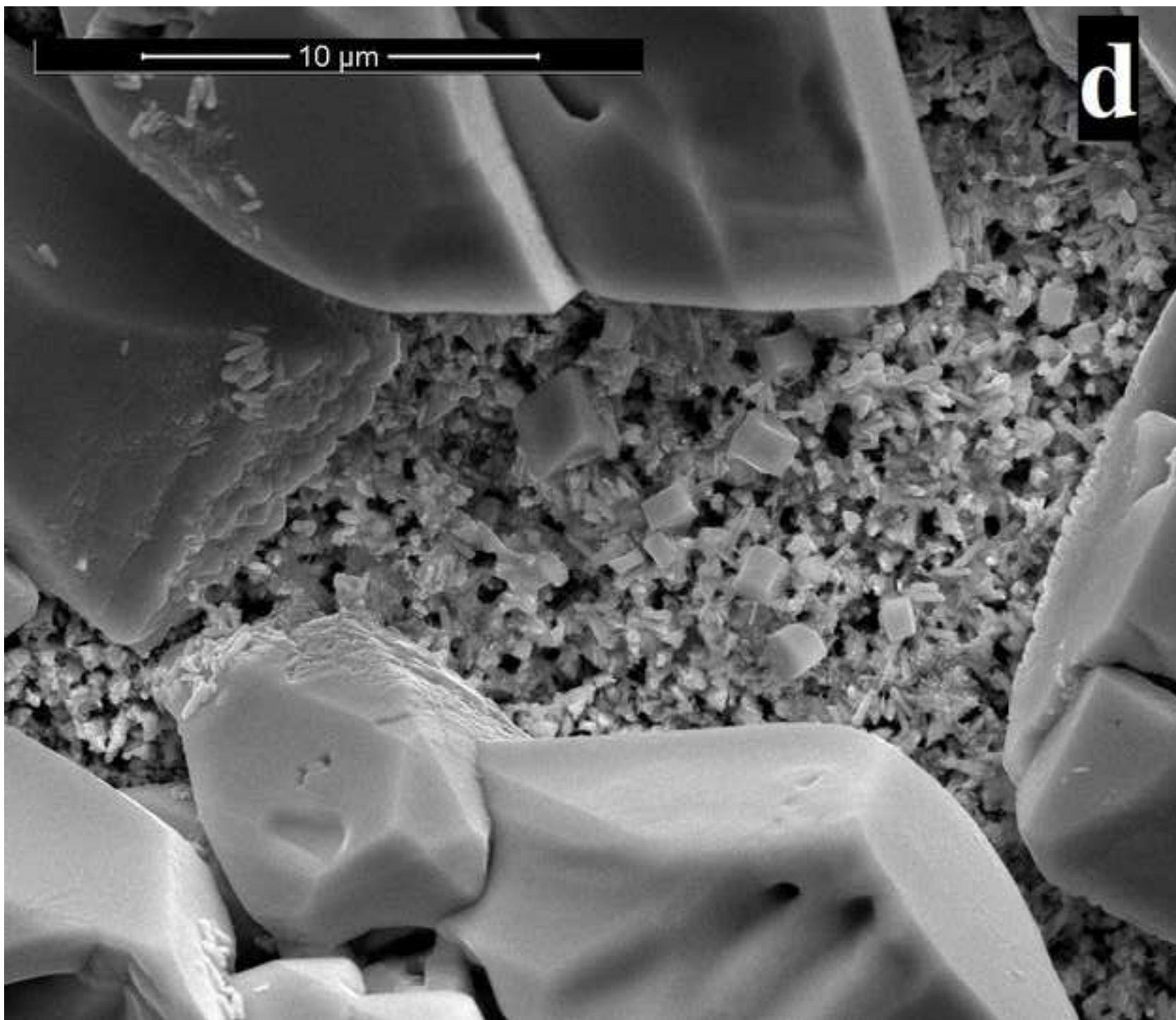


## Figure Captions

**Figure 1** – Rectangular current pulses, with relative and voltage response, powering the electrochemical cell for depositing a lead layer on sputtered gold film covering one side of the template . a) step1, b) step 2, c) step 3. Precursor solution is changed at the end of each step

**Figure 2** – (a) Rectangular current pulses, with relative and voltage response, powering the electrochemical cell for depositing lead nanowires inside the pore of a polycarbonate membrane acting as a template and voltage response. (b-d) Typical morphology of the as-prepared lead nanostructure array at different magnifications.

**Figure 3** – Typical X-ray diffraction patterns of a) as-prepared lead nanostructure array, b) porous mass after cycling under constant current up to end of life

**Figure 4** – Electrochemical performance of nanostructured lead acting as a negative electrode of an electrochemical cell simulating a lead acid battery operating at  $25\pm 2$  °C and 10C, a) First charging and discharging curves: b) Charging and discharging curves; d) Cycling efficiency on discharging of nanostructured

**Figure 5** - Electrochemical performance of nanostructured lead acting as a negative electrode of an electrochemical cell simulating a lead acid battery operating at  $25\pm 2$  °C and 1C, a) First charging and discharging curves: b) Charging and discharging curves; d) Cycling efficiency on discharging of nanostructured

**Figure 6** – Contact angle measured on: (a) as prepared electrode (b) electrode after 50 charge/discharge cycles.

**Figure 7** – SEM image of lead nanostructured electrode after 200 cycles at 10C at the end of charge.

**Figure 8** – Comparison of the morphology of negative nanostructured electrodes after cycling at different C-rate (at the end of discharge): a) 1C after 450 cycles (end of the life), b) 10C after 1500 cycles; c) 1C after 50 cycles, d) 10C after 50 cycles.